

AD-A262 025



2

AMBIENT-ATMOSPHERE COMPATIBLE  
SUPERCONDUCTING FULLERENES

DTIC  
ELECTE  
MAR 24 1993  
S C D

Contract #DASG60-92-C-0087

February 22, 1993

submitted by

Dr. T.A. Miller

Materials and Electrochemical Research (MER) Corporation

7960 South Kolb Road

Tucson, AZ 85706

(602) 574-1980

**DISTRIBUTION STATEMENT A**

Approved for public release  
Distribution Unlimited

These SBIR data are furnished with SBIR rights under Contract No DASG60-92-C-0087. For a period of 2 years after acceptance of all items to be delivered under this contract, the Government agrees to use these data for Government purposes only, and they shall not be disclosed outside the Government (including disclosure for procurement purposes) during such period without permission of the Contractor, except that, subject to the foregoing use and disclosure prohibitions, such data may be disclosed for use by support Contractors. After the aforesaid 2-year period the Government has a royalty-free license to use, and to authorize others to use on its behalf, these data for Government purposes, but is relieved of all disclosure prohibitions and assumes no liability for unauthorized use of these data by third parties. This Notice shall be affixed to any reproductions of these data, in whole or in part.

93 3 18 045

93-05716



808

# TABLE OF CONTENTS

I.	INTRODUCTION AND OVERVIEW	1
II.	EXPERIMENTAL PROCEDURE	2
A.	Fullerene Production	2
B.	Protective Overlayers	3
1.	Single Cycle Deposition of Metallic Fulleride Film	5
2.	Multiple Fullerene/Potassium Layers	8
3.	Protective Overlayer Films	8
4.	Thick Protective Barrier - Ni/Fullerene/Potassium Wire	10
5.	CTE measurement	10
C.	In-Cage Dopants	12
1.	Graphite/Metal Composite Rods Preparation	13
2.	Fullerene Formation Process	13
3.	Extraction and Analysis	14
D.	Alternative Dopants	14
E.	Cryogenic Characterization	16
III.	Results	18
A.	Protective Overlayers	19
1.	CTE Measurement	19
2.	Fullerenes Plus Potassium Only	19
3.	Insulating Protection Layers	29
4.	Polymer/Aluminum Protective Multilayer	35
5.	Metallic Protective Layers	37
6.	Nickel Tube Protection	46
B.	In-cage Dopants	46
C.	Alternate Dopants	53
IV.	Discussion and Conclusion	66
A.	Protective Overlayers	66
B.	in-cage Dopants	67
C.	Alternate Dopants	68

St-A per telecon, Mr. Hyndick,  
SDIO/DTIC, Wash., DC 20301  
3-23-93 JK

DTIC QUALITY INSPECTED 1

Accession For	
NTIS CRA&I	<input checked="" type="checkbox"/>
DTIC TAB	<input type="checkbox"/>
Unannounced	<input type="checkbox"/>
Justification	
By	
Distribution/	
Availability Codes	
Dist	Avail and/or Special
A-1	

## List of Figures

- Figure 1. Schematic of thin film resistivity sample.
- Figure 2. Apparatus for multilayer polymer/metal deposition.
- Figure 3. Coefficient of Thermal Expansion of pure  $C_{60}$  pellet, 93% dense.
- Figure 4. Resistivity of fulleride films during the deposition of alternating layers of fullerenes (100 Å thick) and potassium. The potassium stoichiometry is nominal only.
- Figure 5. Resistivity of fulleride films during the deposition of alternating layers of fullerenes (200 Å thick) and potassium. The potassium stoichiometry is nominal only.
- Figure 6. Resistivity of fulleride films during the deposition of alternating layers of fullerenes (400 Å thick) and potassium. The potassium stoichiometry is nominal only.
- Figure 7. Resistivity of fulleride films during the deposition of alternating layers of fullerenes (1000 Å thick) and potassium. The potassium stoichiometry is nominal only.
- Figure 8. Resistivity of fulleride films during the deposition of alternating layers of fullerenes (1000 Å thick) and potassium plotted as a function of time. Resistance was monitored while the chamber was held in vacuum for two hours.
- Figure 9. Test of fullerenes as a protective overlayer for doped fullerene films. Potassium thickness is nominal.
- Figure 10. Test of Si as a protective overlayer for doped fullerene films. Potassium thickness is nominal.
- Figure 11. Test of SiO as a protective overlayer for doped fullerene films. Potassium thickness is nominal.
- Figure 12. Test of  $CaF_2$  as a protective overlayer for doped fullerene films. Potassium thickness is nominal.
- Figure 13. Test of polymer as a protective overlayer for doped fullerene films. Potassium thickness is nominal.
- Figure 14. Resistivity record of polymer/Al multilayer deposition. Potassium thickness is nominal.
- Figure 15. Resistivity record of 5000 Å Al overlayer deposition. Potassium thickness is nominal.
- Figure 16. Resistivity record of 2000 Å Al overlayer deposition. Potassium thickness is nominal.
- Figure 17. Resistivity record of 1000 Å Al overlayer deposition. Potassium thickness is nominal.
- Figure 18. Resistivity record of 600 Å Al overlayer deposition. Potassium thickness is nominal.
- Figure 19. Resistivity record of Cu overlayer deposition. Potassium thickness is nominal.
- Figure 20. Resistivity record of Ag overlayer deposition. Potassium thickness is nominal.

- Figure 21. Magnetization of arc burned  $\text{Ag}_1\text{C}_{60}$  sample as a function of a) temperature using a 100 Oe field, and b) as a function of field at 10 K.
- Figure 22. Magnetization of arc burned  $\text{La}_1\text{C}_{60}$  sample as a function of a) temperature using a 100 Oe field, and b) as a function of field at 10 K.
- Figure 23. Magnetization of arc burned  $\text{La}_5\text{C}_{60}$  sample as a function of a) temperature using a 100 Oe field, and b) as a function of field at 10 K.
- Figure 24. Magnetization of HIPed  $\text{Zn}_6\text{C}_{60}$  sample as a function of temperature in a quartz plug holder.
- Figure 25. Magnetization of HIPed  $\text{Zn}_6\text{C}_{60}$  sample as a function of temperature in a quartz gap holder.
- Figure 26. Magnetization of heat treated  $\text{Th}_{0.75}\text{C}_{60}$  as a function of temperature.
- Figure 27. Magnetization of heat treated  $\text{Th}_{1.5}\text{C}_{60}$  as a function of temperature.
- Figure 28. Magnetization of heat treated  $\text{Th}_3\text{C}_{60}$  as a function of temperature.
- Figure 29. Magnetization of heat treated  $\text{Th}_{0.75}\text{C}_{60}$  at higher temperatures.
- Figure 30. High field magnetization of heat treated  $\text{Th}_{0.75}\text{C}_{60}$  at various temperatures.
- Figure 31. Low field magnetization of heat treated  $\text{Th}_{0.75}\text{C}_{60}$  at various temperatures.
- Figure 32. Magnetic susceptibility of heat treated  $\text{Th}_{0.75}\text{C}_{60}$  at various temperatures.

#### List of Tables

- Table I. Protective Overlayer Compositions. Type and Deposition Method.  
Table II. Alternate Dopants Tested. Reasons for Testing and Treatments.  
Table III. Values of resistivity and nominal potassium stoichiometry at resistivity minimum during doping.  
Table IV. Deposition thicknesses and cryogenic resistivity ratios for metallic overlayers.  
Table V. EDS test of solid products for metal dopants. Yes means metal was detected in the extract.

## I. INTRODUCTION AND OVERVIEW

The goal of this Phase I project was to evaluate different methods to produce ambient-atmosphere compatible superconducting fullerenes. Three approaches toward this goal were surveyed, 1) protective overlayers, 2) in-cage dopants, and 3) alternate dopants. A source of electrons for the conduction band derived from the lowest unoccupied molecular orbitals, other than reactive alkali metals is desired. All three methods demonstrated interesting and tantalizing results.

Potassium doped fullerene films were produced in our high vacuum (HV) deposition chamber. Difficulties in transporting potassium from the shipping container to the deposition chamber were solved by the use of a kerosene/isopropanol bath. Measuring electrical resistivity proved to be an effective method of monitoring the doping process. Protective overlayers of doped fullerene films were formed with various combinations of electrical conductors and insulators. The electrically insulating layers could be tested immediately at MER, while the metallic layers required cryogenic measurements. Aluminum showed promise as a protective layer in the sense that it prevented contamination in ambient atmosphere conditions. However the test for superconductivity failed due probably to impurities incurred during the deposition in the HV chamber, rather than impurities being transported through the aluminum to the fulleride film.

The in-cage dopant samples were prepared by using hollow graphite rods filled with the dopant as the feed rod in the electric arc fullerene production process. Alternate

dopants were prepared by solid state reaction in a hot isostatic press or in an argon furnace. Both the in-cage dopants and alternate dopants showed tantalizing phase transitions based on the magnetometer measurements by our colleagues at Ames. These measurements, strongest for Th doped samples, indicated flux expulsion at temperatures as high as 100 K. These very exciting preliminary results must be verified by electron transport measurements in purified superconducting phase material.

## II. EXPERIMENTAL PROCEDURE

### A. Fullerene Production

For the purposes of these experiments, fullerenes were procured from MER's Huffman-Krättschmer (H-K) fullerene production facility. With the H-K technique, an electric arc is passed between two graphite electrodes and carbon soot is produced from the graphite in the intense heat of the arc. In typical production runs, between 10% and 20% of the soot is carbon in fullerene form. These fullerenes are extracted from the remainder of the soot by dissolving in toluene, which is a fullerene solvent but not a graphite solvent. The toluene is evaporated from the fullerenes leaving behind fullerenes composed approximately of 85%  $C_{60}$ . Most of the remaining 15% is  $C_{70}$  with small amounts of  $C_{84}$  and higher order fullerenes. Fullerenes of different molecular weights can be chromatographically separated in an alumina column using hexane as an eluant. The raw materials used in this project were primarily  $C_{60/70}$  from the toluene extraction, and purified  $C_{60}$  from the hexane separation.

## B. Protective Overlayers

All of the thin film samples utilized glass substrates which were cut from microscope slides. In the later part of the experiment, the glass substrate size was changed from 0.219" x 1" to 0.094" x 0.813", as shown in Figure 1, to enable the resistivity measurement in small bore cryostats. Starting out with precleaned microscope slides, substrates of the above sizes were cut by a diamond saw, then sonicated in a soap solution, rinsed with distilled water and sonicated again in isopropanol for about 15 minutes. Each substrate's central area was masked with aluminum foil, during deposition of silver pads for electrical contact. The unmasked portion was coated with 500 Angstroms of Ni to improve adhesion, then 2000 Angstroms of Ag. Wires were attached to the Ni/Ag electrode pads by low temperature indium soldering. Prior to fullerene deposition, substrates were cleaned again by RF plasma as needed. Initial experiments, described in section 1 and 2 below, established deposition parameters for producing metallic fullerenes. Once these procedures were established, overlayers were applied to be tested as protection coatings.

A second geometry to protect the environmentally sensitive fullerenes from air was to incorporate the potassium doped fullerenes at the center of a thick wire. This device was constructed in a sealed nitrogen glove box. Fullerenes and potassium were placed in a nickel tube and the ends were plugged with nickel wire and then welded shut to protect the doped fullerenes from the atmosphere. The sealed wire was removed from the glove box and heat treated at 200°C for 60 hours to intercalate the potassium into the  $C_{60}$  lattice.

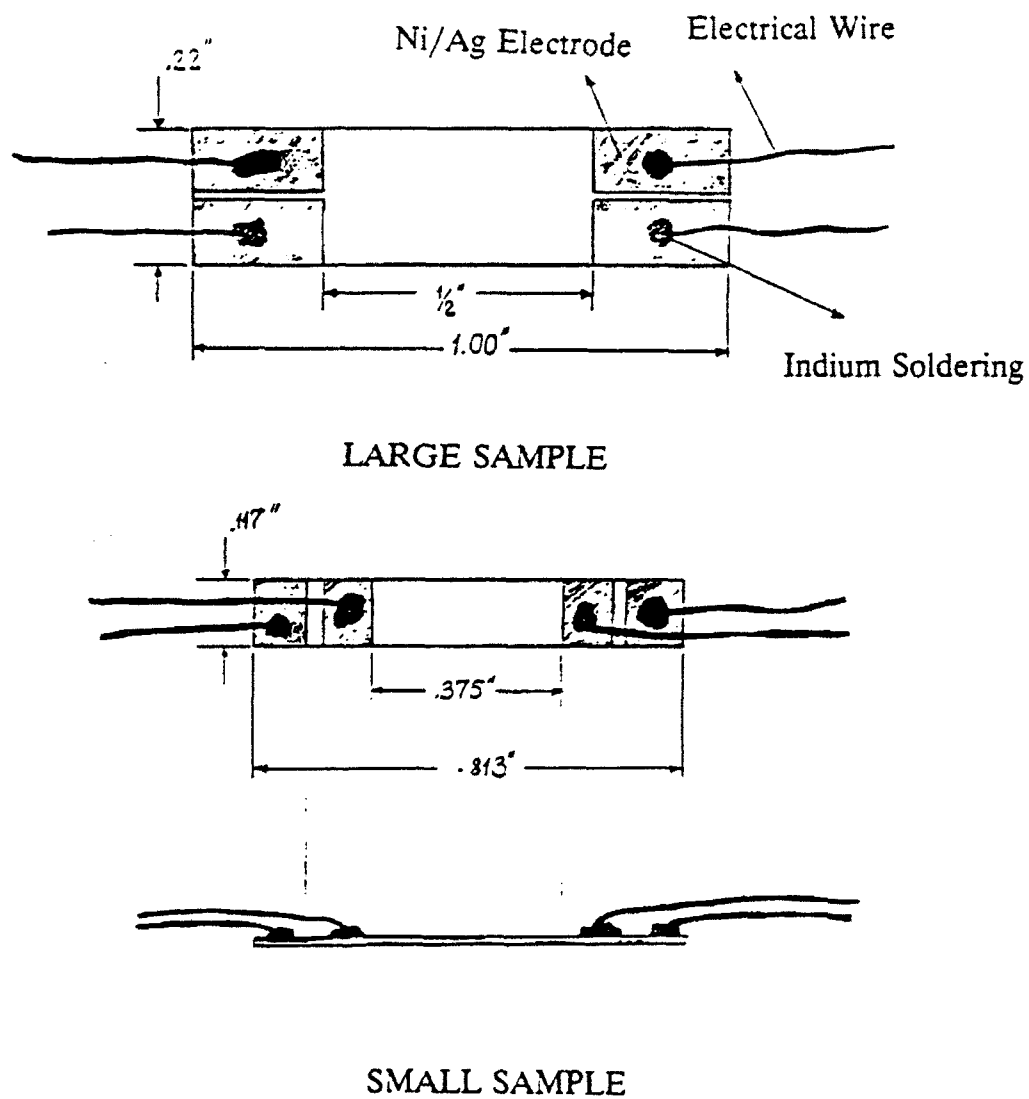


Figure 1. Schematic of thin film resistivity sample.

## 1. Single Cycle Deposition of Metallic Fulleride Film

Two resistive heating sources, one for fullerene and the other for K, were set up side by side to provide equal line-of-sight trajectories toward the substrate. The substrate was held face down, above the sources, about 6 inches to 12 inches away. The substrate-to-source distance was one of the controlled parameters of the experiments.

One of the major processing problems was handling potassium, particularly transferring potassium metal from the storage container to the vacuum chamber. The source of the difficulty is that potassium forms oxides and hydroxides very readily in air. The high reactivity of potassium is the reason the alkali-doped fullerides are so sensitive in ambient air, and the reason to pursue this Phase I project.

Initially, potassium was taken out of its container in an inert gas glove bag, immediately covered by liquid nitrogen for transporting into the vacuum chamber. This process diminished contamination of the potassium but not sufficiently to produce pure films. Subsequently, kerosene was used instead of liquid nitrogen. The potassium could be transferred to a crucible and covered with kerosene with minimal contamination of the potassium surface. The protected potassium could then be transported to the vacuum chamber where the kerosene was evaporated as the chamber was evacuated. A further refinement of the kerosene protection scheme was to add a few drops of isopropanol to the kerosene. The effect of the isopropanol was to wash any remnant contaminants from the

surface of the potassium.

With vacuum in the  $10^{-6}$  Torr range, the fullerenes were evaporated onto the glass substrate from a resistively heated tantalum boat. Fullerene thickness was continuously monitored by a pre-calibrated quartz crystal thickness monitor which has a resolution to 0.1 of an angstrom. The substrate's resistivity was monitored by a multimeter connected to the soldered wires on the substrate. When the fullerene deposition ended, a shutter was closed to cover the substrate. To evaporate any remaining kerosene, the power was slowly increased in the K source. The shutter was a double precaution since most of the kerosene was evaporated during the initial evacuation of air. After all the kerosene was evaporated, the shutter was opened, power increased to the K crucible and K deposition was indicated on the thickness monitor. K evaporation was carried out at different rates to find the effect of diffusion rate on the formation of the superconductive phase,  $K_3C_{60}$ .

During continuous potassium evaporation, the potassium doping can be directly monitored by measuring the resistivity of the films.  $C_{60}$  is an insulator so the resistance of the film is initially unmeasurably high. As the potassium is added, the resistance is expected to drop to a minimum as the potassium concentration approaches  $K_3C_{60}$ , the superconducting phase. If the potassium deposition and diffusion is continued, the concentration approaches  $K_6C_{60}$ , and insulating phase, and the resistance is expected to rise to a maximum. If potassium deposition continues still, then the resistance is expected to drop as conduction becomes dominated by the metallic potassium.

With the quartz crystal monitor we were able to measure a relative thickness of potassium. The crystal monitor was first used to measure the thickness of the fullerene deposition. Then without changing the crystal (which would have required breaking vacuum) the potassium deposition was measured. The signal from the quartz crystal thickness monitor depends on the total mass deposited, on density, and on the shear modulus of the deposited material. Usually the dependence on density and shear modulus is lumped into a single term called the Z-ratio which typically ranges from 0.1 to 3 for common materials. When the Z-ratio of a material is not known, as was the case for both the fullerenes and potassium, it can be determined by performing test depositions and measuring the actual thickness and back-calculating the Z-ratio. This procedure was followed for the fullerenes (the Z-ratio was close to 1), but could not be performed with potassium because of the reaction in air. Additionally, even if the Z-ratio were known, the potassium diffuses into the fullerenes so readily on deposition, that the bulk Z-ratio would not be valid. In much of the work reported below, we report a nominal potassium thickness which is the reading of the quartz crystal monitor when the Z-ratio is taken to be one.

During the course of these depositions, the goal was to achieve a resistivity of 2 milli  $\Omega$ -cm. This is the value reported in the literature as corresponding to the superconducting phase. Unfortunately, the lowest resistivity we typically achieved was 10 m $\Omega$ -cm, well above the desired value. Occasionally our measured resistivity dropped to 3 to 5 m $\Omega$ -cm. As later measurements indicated, the high base resistivity did not permit the superconducting phase

transition to take place. We conjecture that despite the base pressures in the  $10^{-6}$  Torr range in our deposition chamber, there was still contamination of the very reactive potassium. Nevertheless, because of the metallic conduction in the doped films, we were still able to evaluate the electrically insulating protective overlayers by observing the resistance as the chamber was filled with air.

## **2. Multiple Fullerene/Potassium Layers**

The deposition procedure is generally the same as the previous section, except more than one fullerene/K bilayer were deposited onto the glass substrate. The goal was to test whether the doping and subsequent drop in resistance was diffusion limited. The thickness of fullerene layers varied from 100, 200, 500, 1000 and 2000 Angstroms. Potassium was evaporated following each fullerene deposition until a resistivity minimum was achieved. There were always an odd number of depositions, alternating fullerenes and potassium, with the first and last deposition being a fullerene deposition.

## **3. Protective Overlayer Films**

The main objective of this portion of the experiment was to find an effective overlayer that could protect the fullerene/K superconductive film from the atmosphere. Fullerenes were deposited to a thickness of typically  $0.2\ \mu\text{m}$  and  $1\ \mu\text{m}$ , and then potassium was deposited until the resistance minimum indicated optimal doping. After

doping with potassium, the protective overlayers were deposited. The overlayers can conceptually be divided into insulators and conductors. The conductive overlayers caused an electrical short of the sample and any rise in resistance of the doped fullerene film as the chamber fills with air is masked by the conductivity of the metallic overlayer itself. Samples with metallic protective overlayers had to be sent to our colleagues at Ames for cryogenic evaluation. On the other hand, the insulating overlayers could be evaluated immediately upon exposure to air. A third type of protective overlayer is a multilayer of insulating and conducting layers. This type can be evaluated as the insulators are, that is to say, immediately, if an insulating layer is adjacent to the doped fullerene film. The multilayer overlayer was used to establish the effectiveness of Al as a protective barrier.

**Table I: Protective Overlayer Compositions, Type and Deposition Method**

<b>Composition</b>	<b>Type-Insulative (I) or Conductive (C)</b>	<b>Deposition Method</b>
Fullerenes	I	resistive heating sublimation
Si	I	electron beam evaporation
SiO	I	resistive heating sublimation
SiO <sub>2</sub>	I	electron beam evaporation
CaF <sub>2</sub>	I	resistive heating evaporation
Polymer	I	see text
Polymer/Al	I*	see text/resistive heating evaporation
Ag	C	resistive heating evaporation
Cu	C	resistive heating evaporation
Al	C	resistive heating evaporation

\* Evaluated as an insulating layer, but contains an electrically isolated metallic layer(s).

The overlayer compositions and deposition techniques are summarized in Table I. The polymer layer was deposited in liquid monomer form, and then polymerized by electron beam bombardment.

To deposit the polymer/Al multilayer, a special configuration was required as depicted in Figure 2. The substrate was placed in a four stage rotating fixture. The first stage was the fullerene and potassium deposition. The second stage was monomer deposition. The third stage was monomer curing and the fourth stage was aluminum deposition. After the doped fullerenes were deposited, depositions at stages 2, 3 and 4 were repeated several times.

#### **4. Thick Protective Barrier - Ni/Fullerene/Potassium Wire**

A Ni tube (2" long, 3/32" I.D., 0.020" wall) with one end weld-closed, was used as the reaction chamber as well as a means of protection for the atmosphere sensitive  $K_3C_{60}$ . In a neutral atmosphere (Nitrogen), a stoichiometry amount of K and  $C_{60}$  were put into the Ni tube so that they would form  $K_3C_{60}$  after being reacted. The tube was then evacuated, welded, heated to about 200°C, for 60 hours, to allow K to diffuse into the  $C_{60}$  matrix. The material was compacted by mechanical swaging prior to testing.

#### **5. CTE measurement**

In a long term situation, a protective overlayer will need to be able to withstand repeated cryogenic thermal cycling. Other than adhesion, the most important material parameter is the coefficient of thermal expansion (CTE) which should match that of the

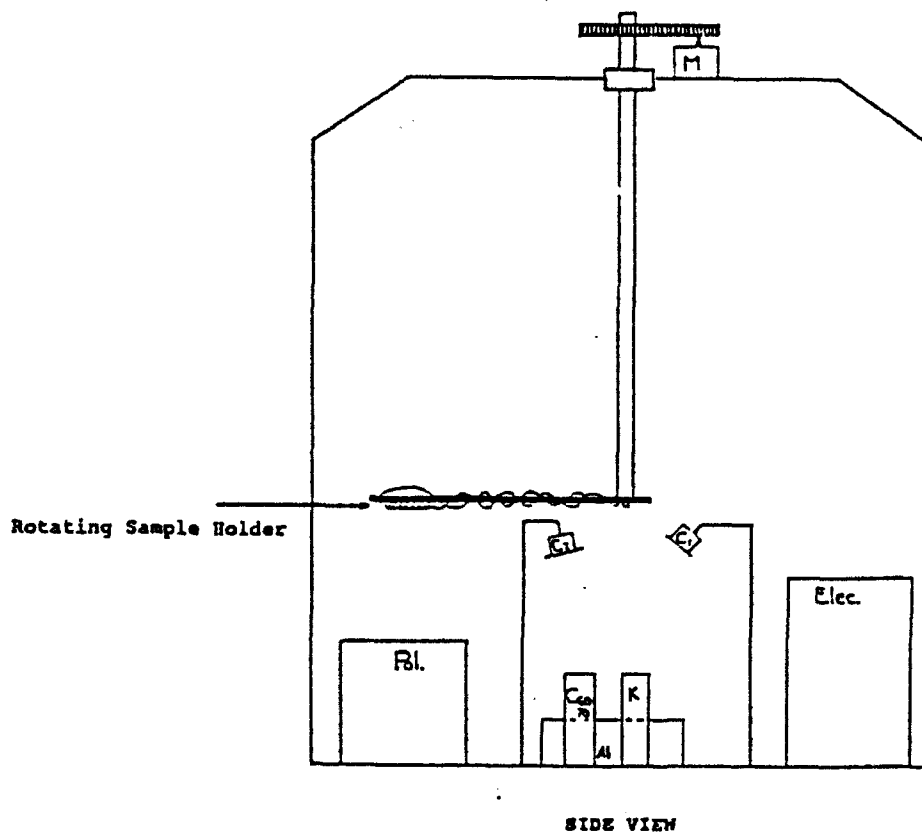
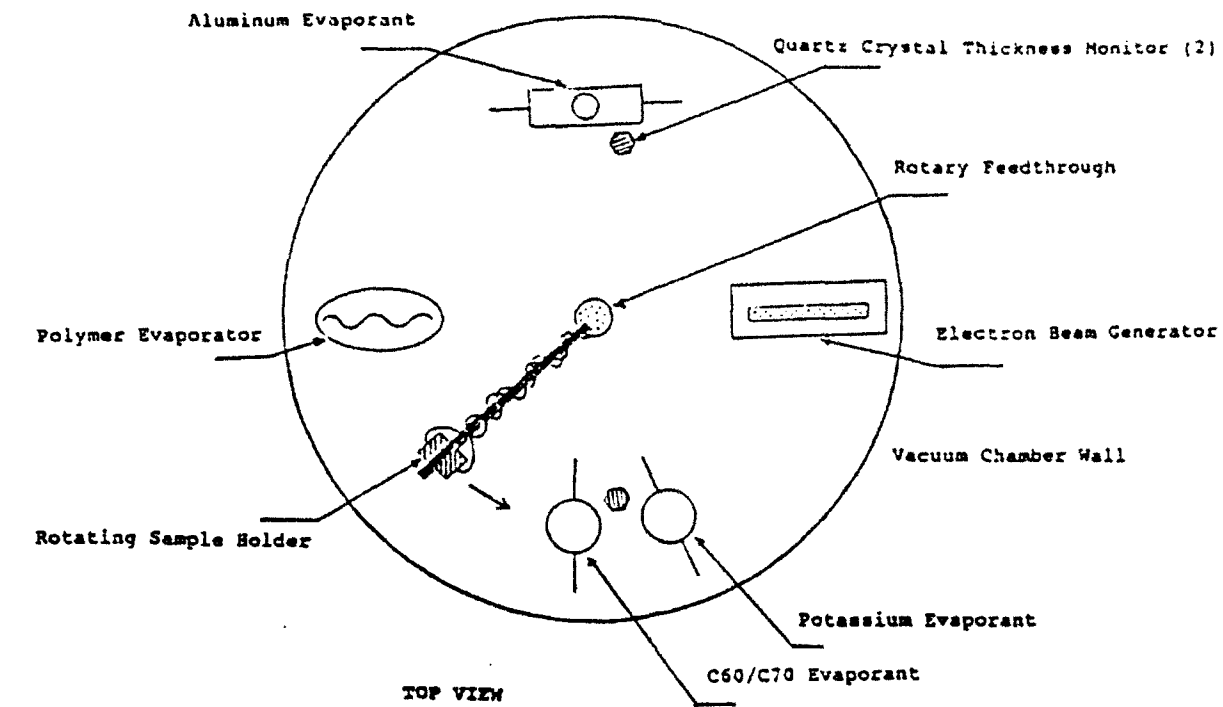


Figure 2. Apparatus for multilayer polymer/metal deposition.

fullerenes as much as possible. To determine CTE, a pellet of  $C_{60}$  was cold pressed to 93% of theoretical density. Using ASTM standard methods, the CTE was measured in a quartz vessel using a quartz rod to transmit the expansion of the sample to a LVDT linear position detection system. An unsheathed low temperature thermocouple was within 2 mm of the sample. The atmosphere was He gas under a controlled flow rate to eliminate contamination with frozen gases from ambient air. The sample was measured cryogenically in a liquid nitrogen dewar system and transferred to a small furnace for a high temperature CTE measurement.

### C. In-Cage Dopants

Dopants inside the fullerene cages have been targeted as a potential approach to superconductivity because of the inherent protection of the dopant provided by the carbon cage. Based on past history with the fullerenes, the choice of dopant must be a ready electron donor. The choice of dopant materials was further narrowed by a requirement for separation of the in-cage doped fullerenes from soot and undoped fullerenes. We chose materials with a high bulk magnetic susceptibility with the hope that enough of the magnetic properties of the dopant would translate to the product to enable magnetic separation of the fullerenes. Lanthanum and strontium were chosen as a reasonable combination of low ionization energy, high magnetic susceptibility, and lower cost.  $La_2O_3$  and SrO were chosen as dopants compounds. Discussions with other researchers in the field indicate that the oxygen from these compounds reacts with carbon

in the soot to form CO and CO<sub>2</sub> without noticeably affecting fullerene yield. Silver was also chosen as a lower cost metal for testing of the processing methods.

### **1. Graphite/Metal Composite Rods Preparation**

High strength Poco graphite rods (12" long, ¼" diameter) were drilled axially with an ⅛" diameter hole. La<sub>2</sub>O<sub>3</sub>, SrO, and Ag were individually mixed with graphite cement in the proportion of 1:1, and 5:1, metal:C<sub>60</sub>. All carbon atoms in the composite rod were accounted for in this calculation, including graphite rod, graphite powder and carbon based epoxy. The rod was filled with cement and dopant mixture and allowed to cure. The rod was heat treated in vacuum at 600°C for two hours, to remove moisture and volatile organics. To ensure that the graphite cement did not affect the fullerene formation, a baseline rod with only graphite cement in the core (no metal) was successfully used to produce fullerenes at a typical efficiency.

### **2. Fullerene Formation Process**

Once the rods were prepared, soot was produced using the previously described H-K method. The graphite/metal rods were vaporized by an arc power supply setting at about 100 Amperes and voltage between 25-30 V. Prior to the reaction, the chamber was evacuated and purged with Ar gas several times, then backfilled with He (to about 23.5" Hg of vacuum). The fullerene soot generated by the reaction was collected for analysis.

### 3. Extraction and Analysis

Metal-fullerene was extracted by using toluene or 1-methyl-2-pyrrolidinone (NMP) as a solvent as previously described (Section IIA). NMP is an alternate solvent to toluene, but dissolves much more of the arc treated soot. NMP was used to test whether the metal atoms were embedded in fullerenes other than the toluene soluble  $C_{60}$ ,  $C_{70}$ , and  $C_{84}$ . The Amray SEM 1200C with Kevex 7000 EDX was used to identify any metal presence within the soot, NMP extracted product, and toluene extracted product. These samples were then shipped to Ames to be tested for superconductivity in the Ames magnetometer.

#### D. Alternative Dopants

The third approach to producing ambient atmosphere compatible superconducting fullerenes was to intercalate less reactive potential deposits. Two approaches were attempted, hot isostatic pressing (HIP) in Ni tubes and heat treatment in Ar atmosphere. A third approach of simultaneous deposition of fullerenes and noble metals was avoided because of low likelihood of success.

Materials were chosen for alternate dopants based on two criteria, that they have low carbide formation energy and/or have a low work function for electron emittance. Because

of its very low carbide formation energy, Th doped samples were not HIPed, but simply heat treated at atmospheric pressure. The dopants chosen, the reasons for choice, and heat treatment conditions are summarized in Table II.

**Table II: Alternate Dopants, Tested, Reasons for Testing and Treatments**

Dopant	Low e work potential (W) or low carbide formation energy (C)	Heat treatment
Hf	W	HIP
Zn	W	HIP
Nb	W	HIP
Zr	C	HIP
Nd	C	HIP
Th	C	600°C, Ar, 6 hours

To make HIP samples, Hf, Zn, Zr, Nd, and Nb, fine-mesh metal powders were ground together with fullerene at 1:1, 1:3 and 1:6, metal atom to  $C_{60}$  molecule ratios. The mixtures were dry-pressed to 2000 psi, contained in Ni tubes with both ends weld-closed, the Hot Isostatic Pressed (HIP) at 1200°C and 20,000 psi. Unfortunately, in this attempt, most of nickel tubes were not collapsed as a result of the HIP. The cause of the failure to collapse could have been that the nickel welds failed to maintain their integrity, which would indicate an uncontrolled process parameter in the HIP. In any case, with dwindling resources, only the sample with the collapsed nickel tube ( $Zn_6C_{60}$ ) was measured in the Ames magnetometer.

The thorium metal was also induced to form a carbide with fullerene with three atomic ratios:  $\text{Th}_x\text{C}_{60}$ ,  $x = 0.75, 1.5, 3$ . However,  $\text{Th}_x\text{C}_{60}$  samples were not hot isostatic pressed, but sintered at  $600^\circ\text{C}$  for six hours in an Ar atmosphere furnace.  $\text{Th}_x\text{C}_{60}$  samples were characterized using the magnometer at Ames.

#### E. Cryogenic Characterization

While some of the protective overlayers could be immediately tested for their protective ability, the metallic overlayers were sent directly to the laboratory of Dr. D.K. Finnemore at the USDOE Ames Laboratory and Iowa State University, Department of Physics, referred to as Ames or Ames Lab elsewhere in this document. The cryogenic characterization of the metallic protective overlayers was a DC measurement of electrical resistance. This was carried out with a standard four probe technique. The four wires are soldered to the silver pads on the sample with indium solder in a straight line down the sample. A known current,  $I_{\text{appl}}$ , runs between the outer two wires through the sample. The voltage,  $V_{\text{samp}}$ , is measured across the inner two wires to measure the resistance of the sample using  $R_{\text{samp}} = V_{\text{samp}} / I_{\text{appl}}$ . This measurement eliminates the inclusion of the resistance of the wire, contact pads, and contact/sample interfaces. Reversing the current and remeasuring eliminates the inclusion of thermopower offsets. The measurements were performed at room temperature ( $R_{\text{rt}}$ ), in a liquid nitrogen bath at 77 K ( $R_{\text{LN}}$ ), and in a liquid helium bath at 4.2 K ( $R_{\text{LHe}}$ ). By using resistance ratios,  $R_{\text{rt}}/R_{\text{LN}}$  and  $R_{\text{rt}}/R_{\text{LHe}}$ , to characterize the samples, rather than a calculated resistivity, geometrical uncertainties are eliminated when comparing samples. When the superconducting transition is above 4.2K,

then the liquid helium resistance ratio  $R_n/R_{LHe}$  is infinity. A non-zero ratio indicates either no superconductivity or an incomplete superconducting transition. Frequently, an incomplete transition is characterized by a low liquid helium resistance ratio in comparison to the liquid nitrogen resistance ratio, particularly if the liquid nitrogen resistance ratio is more than 1. An incomplete transition would be detectable as a non-linear I-V curve.

A different cryogenic measurement is used on powder or small bulk samples. This measurement is performed on a Quantum Design SQUID DC Magnetometer and measures the magnetization moment,  $M$ , of a sample. A pure superconducting material phase is indicated by a diamagnetic signal (the magnetization of the sample opposes the magnetic field). The transition to diamagnetism is readily observed as the sample is cooled below its superconducting transition temperature.

A typical magnetization measurement for a Type II superconductor using a magnetometer is to cool the sample to the lowest temperature possible in zero magnetic field, and to turn on a small field to measure the magnetization of the sample. The magnetization of the sample is then measured as the sample is warmed to above the superconducting transition. This magnetization data is called the zero field cooled (zfc) curve. Then with the applied field still turned on, the sample is cooled again to the lowest temperature, and again the magnetization is measured as the sample is warmed. This data is the field cooled (fc) data since the field was on as the sample is cooled below its transition. Because a Type II superconductor will trap magnetic flux, the zfc data has more

diamagnetism than the fc data. When plotted on the same graph, the zfc curve will be lower than the fc curve. The temperature at which the fc and zfc data join is taken to be the superconducting transition temperature.

A second type of measurement with the magnetometer utilized in this project is the magnetization as a function of field,  $M$  vs.  $H$ , at a fixed temperature. If the sample is above the transition temperature a straight paramagnetic line of  $M$  vs.  $H$  is expected. If the sample is a Type I superconductor below its transition temperature,  $M$  vs.  $H$  is a straight diamagnetic line. If the sample is a Type II superconductor, the  $M$  vs.  $H$  curve looks much like a ferromagnetic hysteresis loop due to the trapping of magnetic flux.

### III. Results

Of the three main approaches to producing ambient atmosphere compatible superconducting fullerenes, 1) protective overlayers, 2) in-cage doping, and 3) alternate dopants, both the protective overlayers and the alternate dopants demonstrated possibilities as successful techniques. The in-cage doping showed less success primarily because of difficulty in separating the fullerenes which contain metal atoms from those which did not. One of the techniques to apply protective overlayers protected the doped fullerenes for more than one hour in air and has the potential to be developed into a permanent protection. One of the alternate dopants, thorium, demonstrated a small magnetic field expulsion characteristic of superconducting material, but further experimentation is required to eliminate the possibility that the magnetic signal is not due to a ferro- or ferri- magnetic

transition. The experimental details are discussed below.

## **A. Protective Overlayers**

### **1. CTE Measurement**

The CTE of a purified  $C_{60}$  (>99.5%) pellet 3 mm in diameter and 8 mm long is illustrated in Figure 3. The most dominating feature is the peak in CTE at  $-40^{\circ}\text{C}$ . This structural phase change is associated with additional degrees of rotational freedom of individual  $C_{60}$  molecules as the solid warms up. This phase change has been verified by other researchers. It is not likely that a material with a matching CTE and protective overlayer properties will ever be available. At this point we can try to match the average CTE over the range of typical cryogenic temperatures. The average CTE, over the range from room temperature to liquid nitrogen temperature, including the peak, is approximately 35 ppm/K. This large average CTE can only be matched by polymer coatings. But at temperatures lower than the peak temperature, the CTE is around 20 ppm/K which is close to that of more robust candidates for a protective overlayer, such as aluminum, silver and copper.

### **2. Fullerenes Plus Potassium Only**

Several depositions were performed initially without the attempt to provide protective overlayers in order to simply characterize the potassium deposition and diffusion, to evaluate contamination from the chamber, and to evaluate fullerenes themselves as a protective layer.

# C60, 93% dense

cte004.wq1

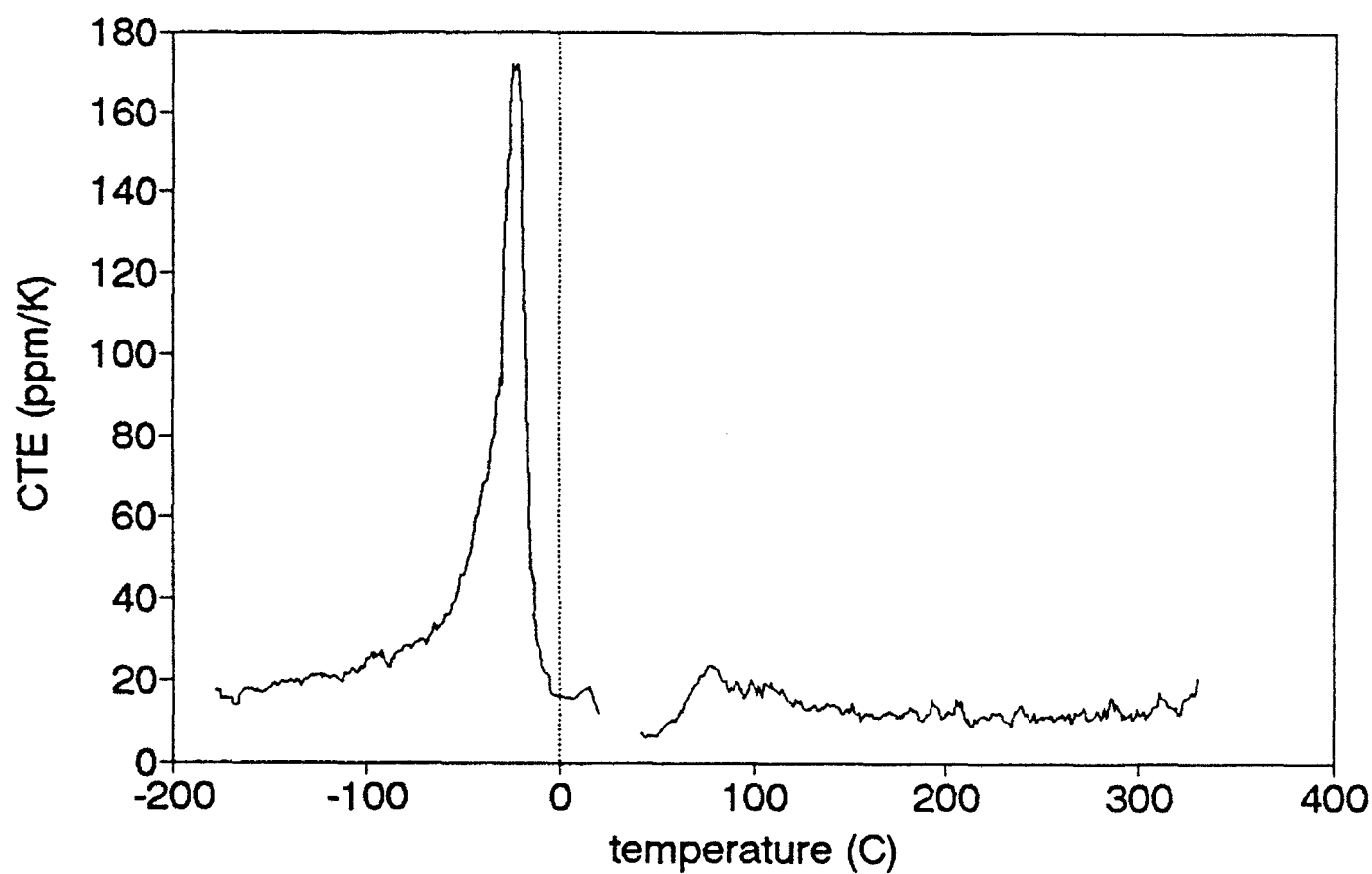


Figure 3. Coefficient of Thermal Expansion of pure C<sub>60</sub> pellet, 93% dense.

In order to evaluate the diffusion of potassium through the fullerenes, a series of multiple deposition experiments was performed using alternating fullerene and potassium layers. Two calculated quantities, resistivity and stoichiometry, are listed in Table III. Again the stoichiometry is nominal because of the systematic errors induced by uncertain Z-ratios for the quartz crystal monitor. These experiments include cycled depositions of fullerenes of 100Å, 200Å, 400Å, and 1000Å thicknesses. As indicated in Figures 4-7, the resistivities are initially high when potassium is first applied (lowest values of  $x$ ). As  $x$  increases, the resistivity drops to a minimum value as the stoichiometry  $K_3C_{60}$  is approached and begins to rise again, at which point the potassium deposition is halted. Following the potassium deposition, a subsequent fullerene deposition will cause the resistivity to change, inducing a higher resistivity as the potassium is drawn from the already doping-level-optimized fulleride film. A subsequent potassium deposition will then again reduce the resistivity. The see-sawing through the "resistivity valley" is particularly evident in the 200Å or the 400Å thicknesses experiments.

**Table III.** Values of resistivity and nominal potassium stoichiometry at resistivity minimum during doping.

Fullerene layer thickness (Å)	Minimum resistivity (ohm-cm)	Minimizing $x$ (nominal) in $K_xC_{60}$
100	.22	3.9
200	.05	5.2
400	.05	5.8
1000	.025	3.7

# Fullerene/Potassium Alternating Deposit 100 Angstrom Full./Low resist. Potassium

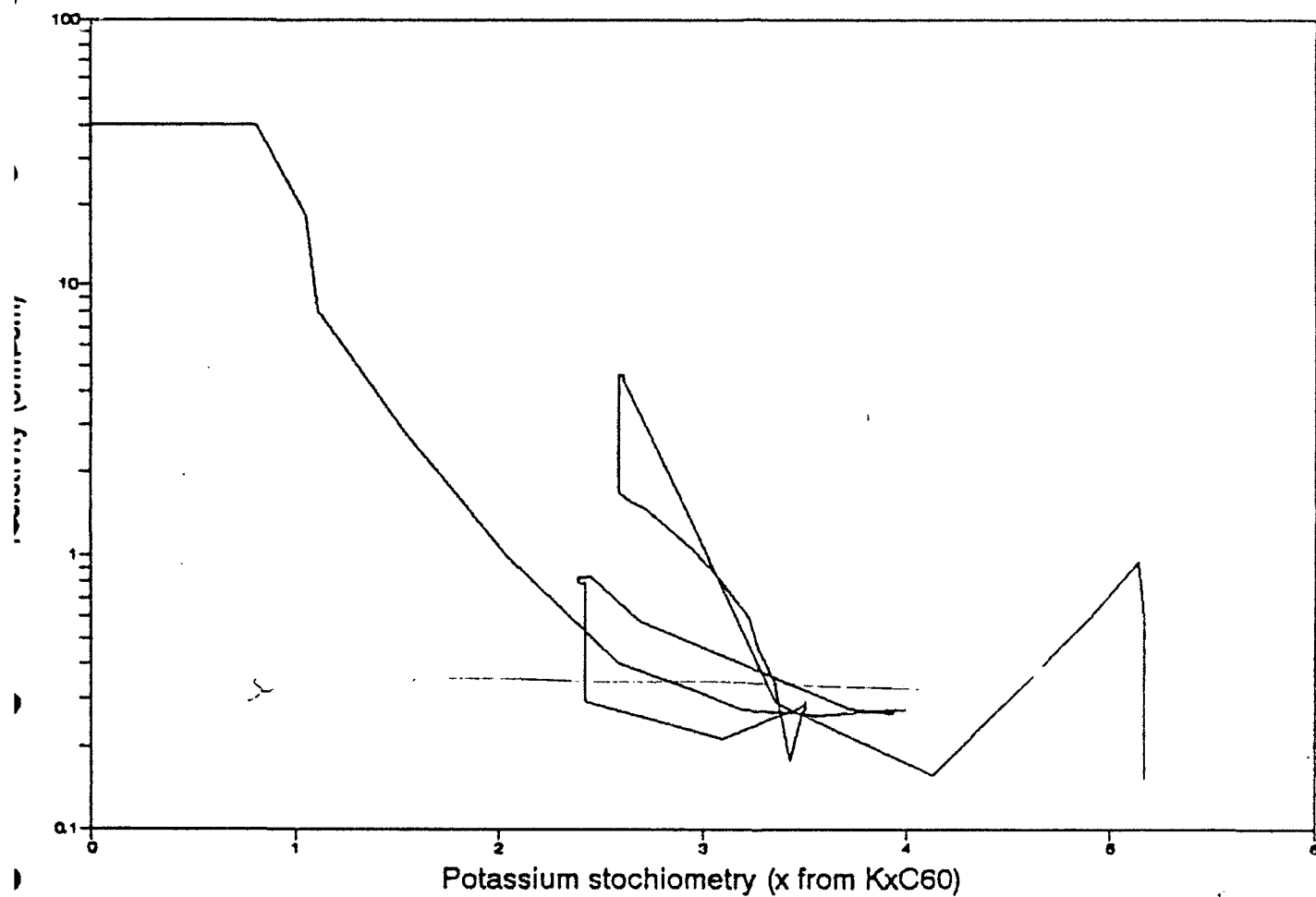


**Figure 4.** Resistivity of fulleride films during the deposition of alternating layers of fullerenes (100 Å thick) and potassium. The potassium stoichiometry is nominal only.

## Fullerene/Potassium Alternating Deposit

200 Angstrom Full./Low resist.Potassium

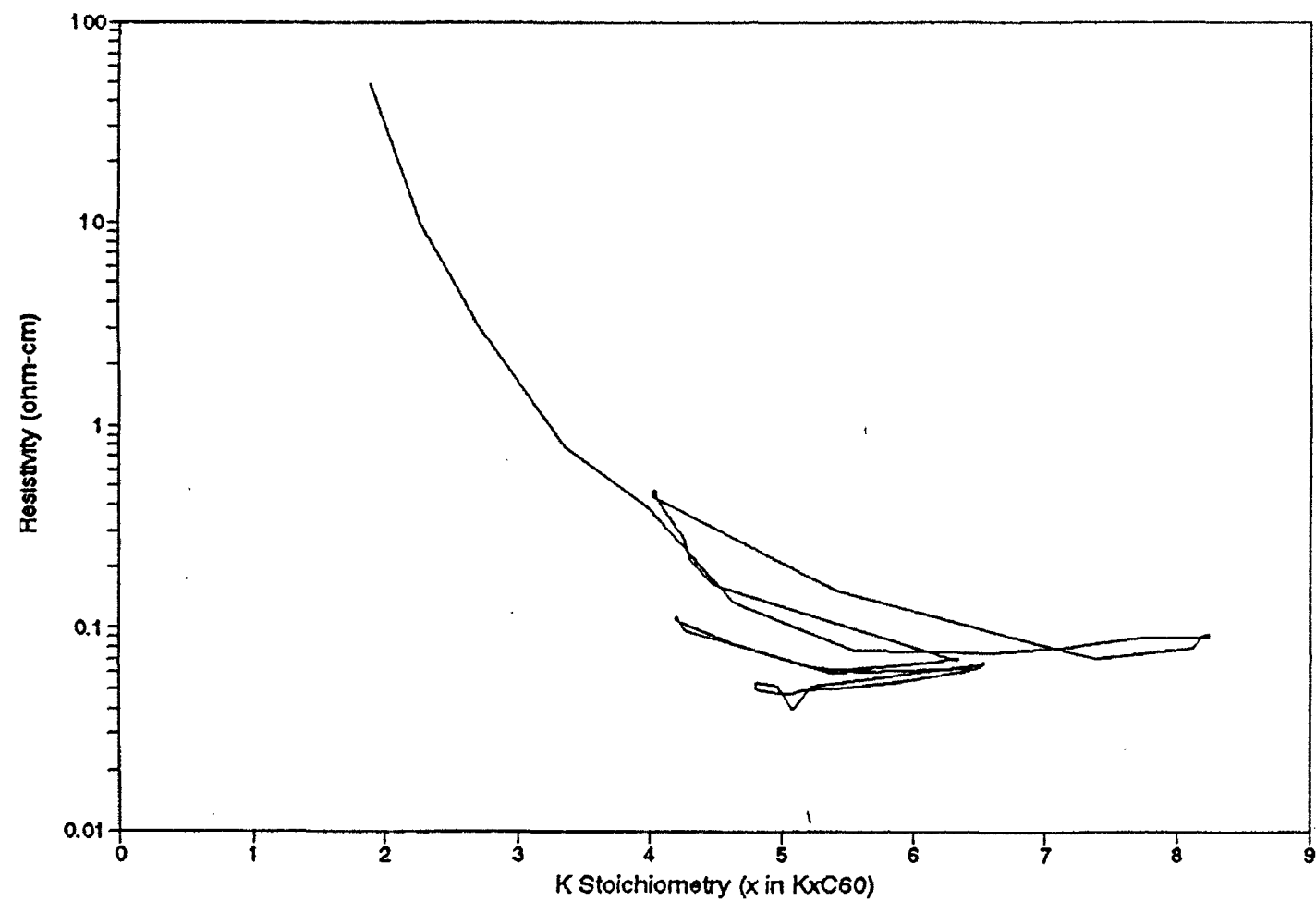


Figure 5. Resistivity of fulleride films during the deposition of alternating layers of fullerenes (200 Å thick) and potassium. The potassium stoichiometry is nominal only.

# Fullerene Potassium Alternating Deposit

400 Angstrom Full./Low Resist.Potassium

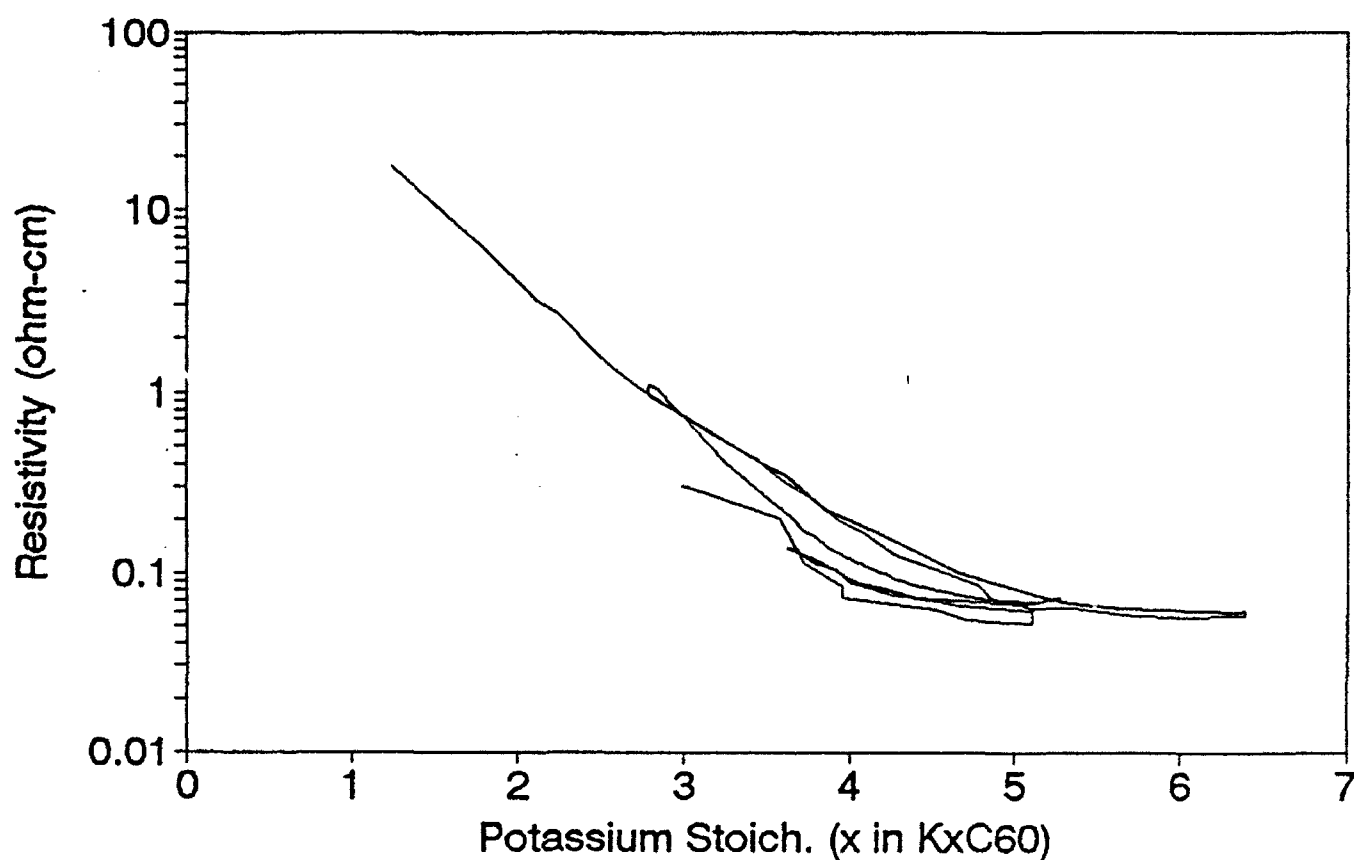


Figure 6. Resistivity of fulleride films during the deposition of alternating layers of fullerenes (400 Å thick) and potassium. The potassium stoichiometry is nominal only.

# Fullerene/Potassium Alternating Deposit

1000 ang. Full./Low Resist. Potassium

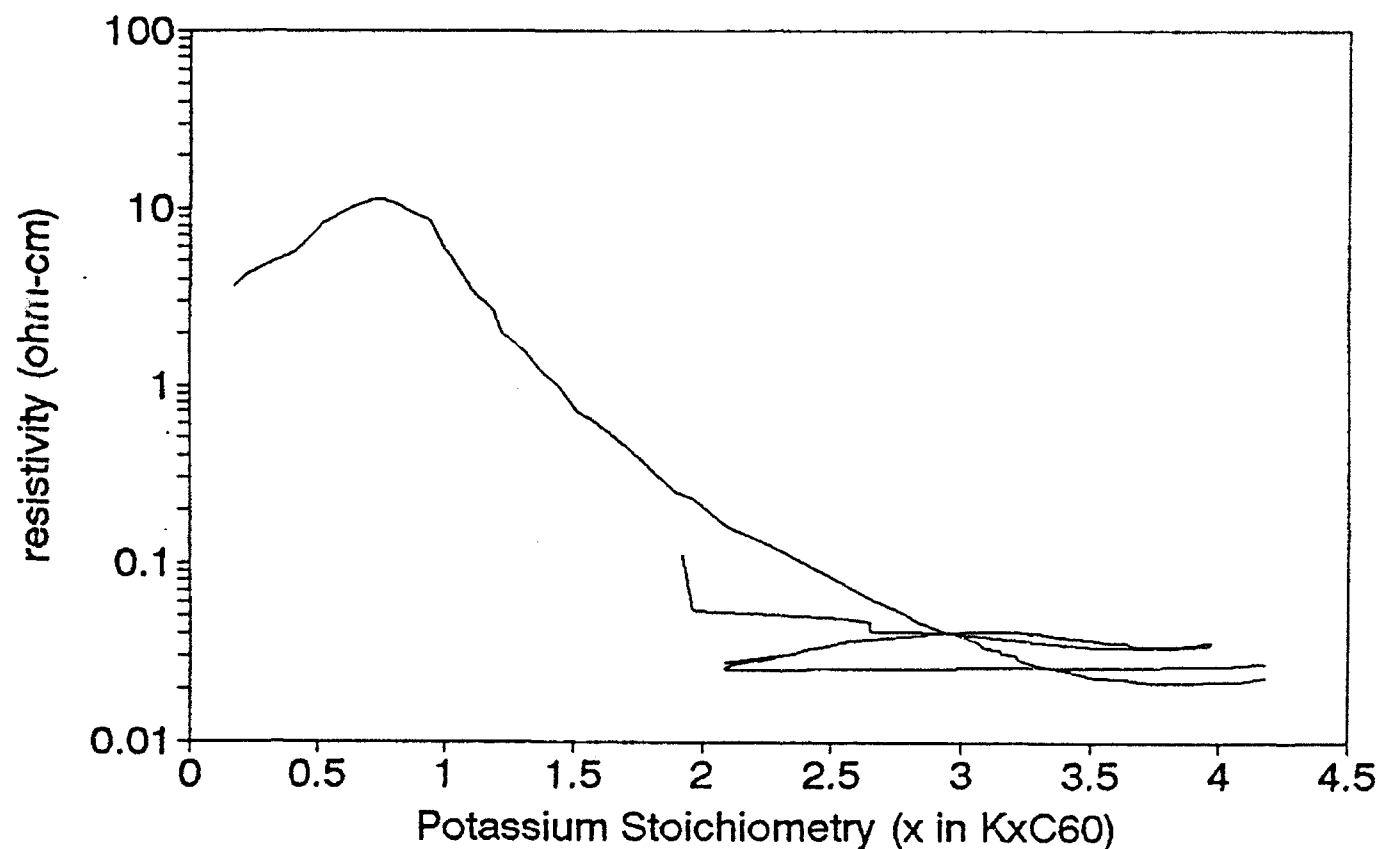


Figure 7. Resistivity of Fulleride films during the deposition of alternating layers of fullerenes (1000 Å thick) and potassium. The potassium stoichiometry is nominal only.

If diffusion limitations are a hindrance to proper doping of the fullerenes, a higher resistance (indicating poor diffusion) would be expected as the layers become thicker. In contrast, the trend is toward lower resistivity as the thickness of each layer increases. This implies that there is a disorder in between each layer of fullerenes that adds to the resistance, and that the thicker layers are less affected by the surface disorder. There is no definite trend in the nominal stoichiometry (last column of Table III) which is an indication of the shallowness of the resistivity minimum and possibly an indication of time dependent processes due to diffusional limitations. To minimize diffusional limitations to accurate doping, the potassium was deposited as slowly as possible during subsequent runs, approximately 0.1 nominal Å/sec.

In order to test contamination from the chamber itself, a fullerene film was doped to a resistance minimum and allowed to stay in the evacuated chamber for several hours. Figure 8 shows the resistivity measured during the deposition of the 1000 Å multilayer as a function of time. The resistivity rose by a factor of four over a period of two hours. The rise in resistivity probably reflects the absorption of oxygen and the loss of free electrons as the potassium reacts with it. The oxygen reaction is probably occurring during the potassium deposition as well but we hope to avoid excessive contamination by depositing protective overlayers as quickly as possible.

The fullerenes themselves were tested as a protection layer. Figure 9 shows the resistance of the film during this test along with the thickness of the fullerenes and nominal

# C60 PROTECTIVE OVERLAYER

C/K/C/K/C, 3 X 1000 Å C60/70, #079070

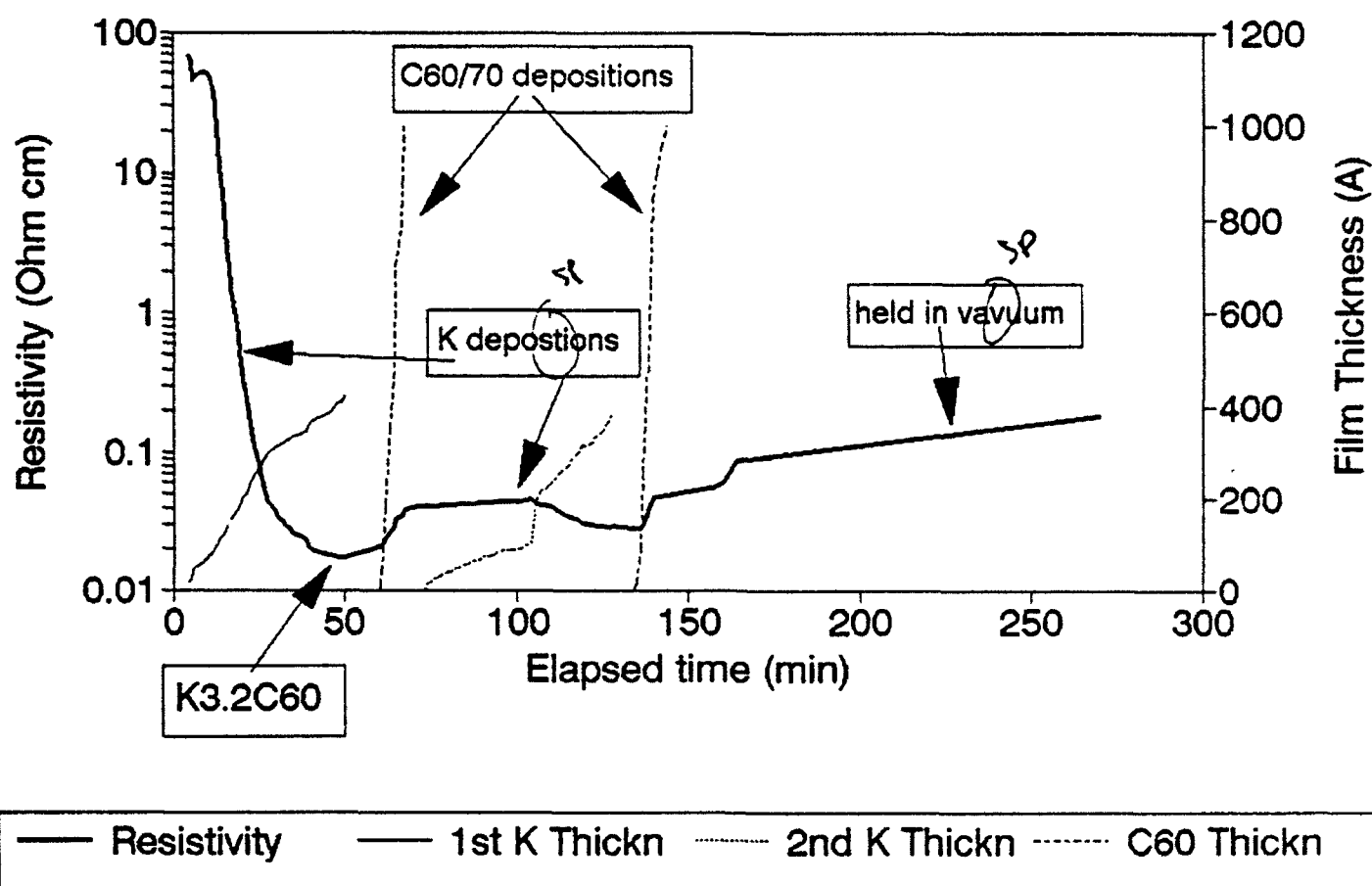


Figure 8. Resistivity of fulleride films during the deposition of alternating layers of fullerenes (1000 Å thick) and potassium plotted as a function of time. Resistance was monitored while the chamber was held in vacuum for two hours.

# C60 PROTECTIVE OVERLAYER

C/K/C/K/C, 2x1000 A C60/70, #079056

3rd C60/70 LAYER 7500 A THICK

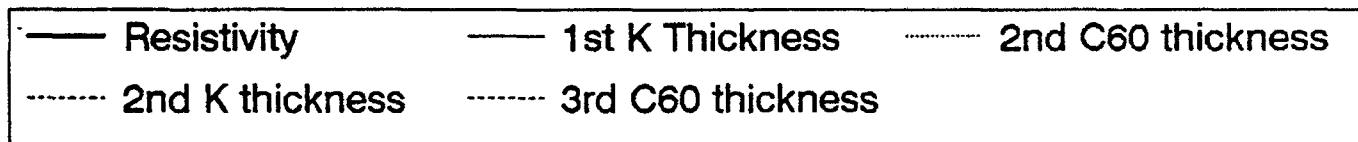
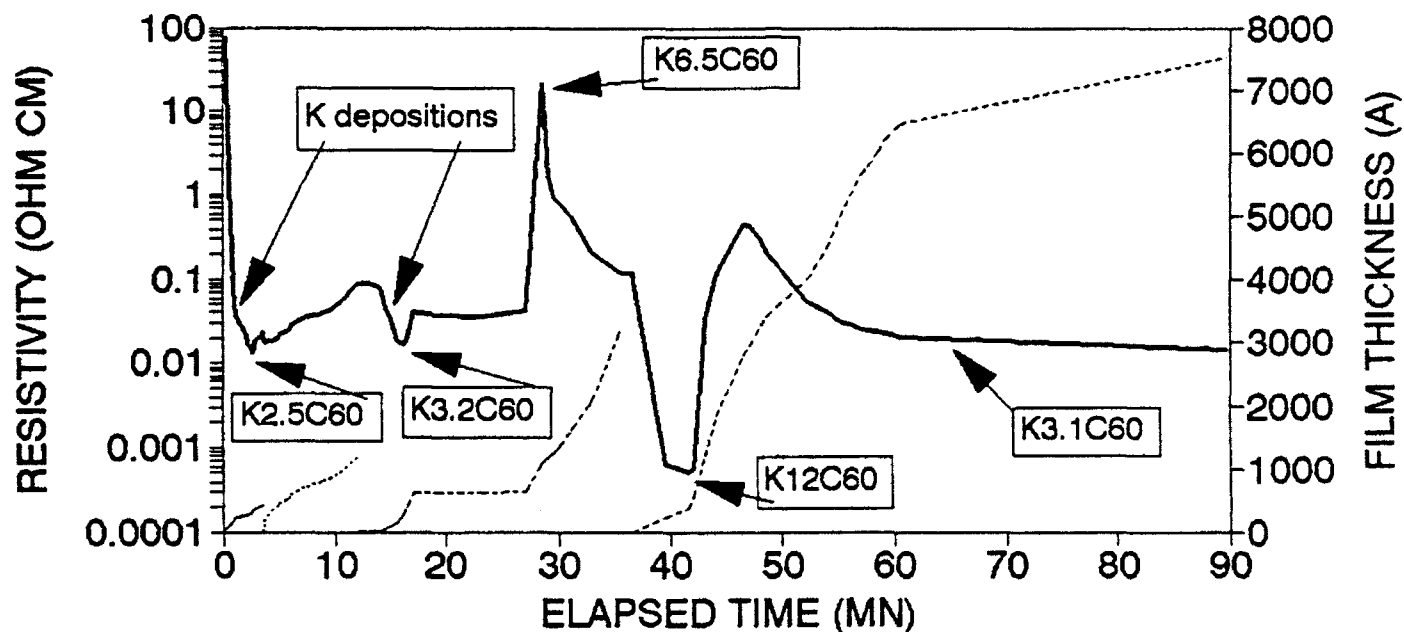


Figure 9. Test of fullerenes as a protective overlayer for doped fullerene films. Potassium thickness is nominal.

thickness of potassium. When the fullerenes were deposited, the resistivity (accounting for the additional thickness of the depositing fullerenes) changed indicating a rediffusion of potassium into the fullerenes. This result contradicts some results in the literature reporting that the  $K_3C_{60}$  phase is stable against diffusion to an undoped phase.

### 3. Insulating Protection Layers

Electrically insulating protection layers were the easiest to evaluate. The resistance of the film was monitored during the process of letting air into the chamber after the run as well as during the doping process. Resistance rising, usually immediately after the air was let in, indicates that the protective overlayer is not doing its job and that the potassium is oxidizing. The resistivity measurement is an immediate evaluation of the protective ability of the electrically insulating film.

Insulating overlayer compositions tested include Si, SiO,  $CaF_2$ , and polymer. The resistivity characteristics of these depositions are plotted in Figures 10, 11, 12, and 13 respectively.  $SiO_2$  was also tested but preliminary depositions demonstrated that the  $SiO_2$  would not adhere to a fullerene surface and could not protect it.

The Si deposition in Figure 10 showed a rise in resistance immediately upon Si deposition. This indicates that Si cannot be used as a protective since the potassium in the fullerene film has an affinity for the Si overlayer.

# C60 PROTECTIVE OVERLAYER

C/K/C/K/C, 3 X 1000 A C60/70, #079070

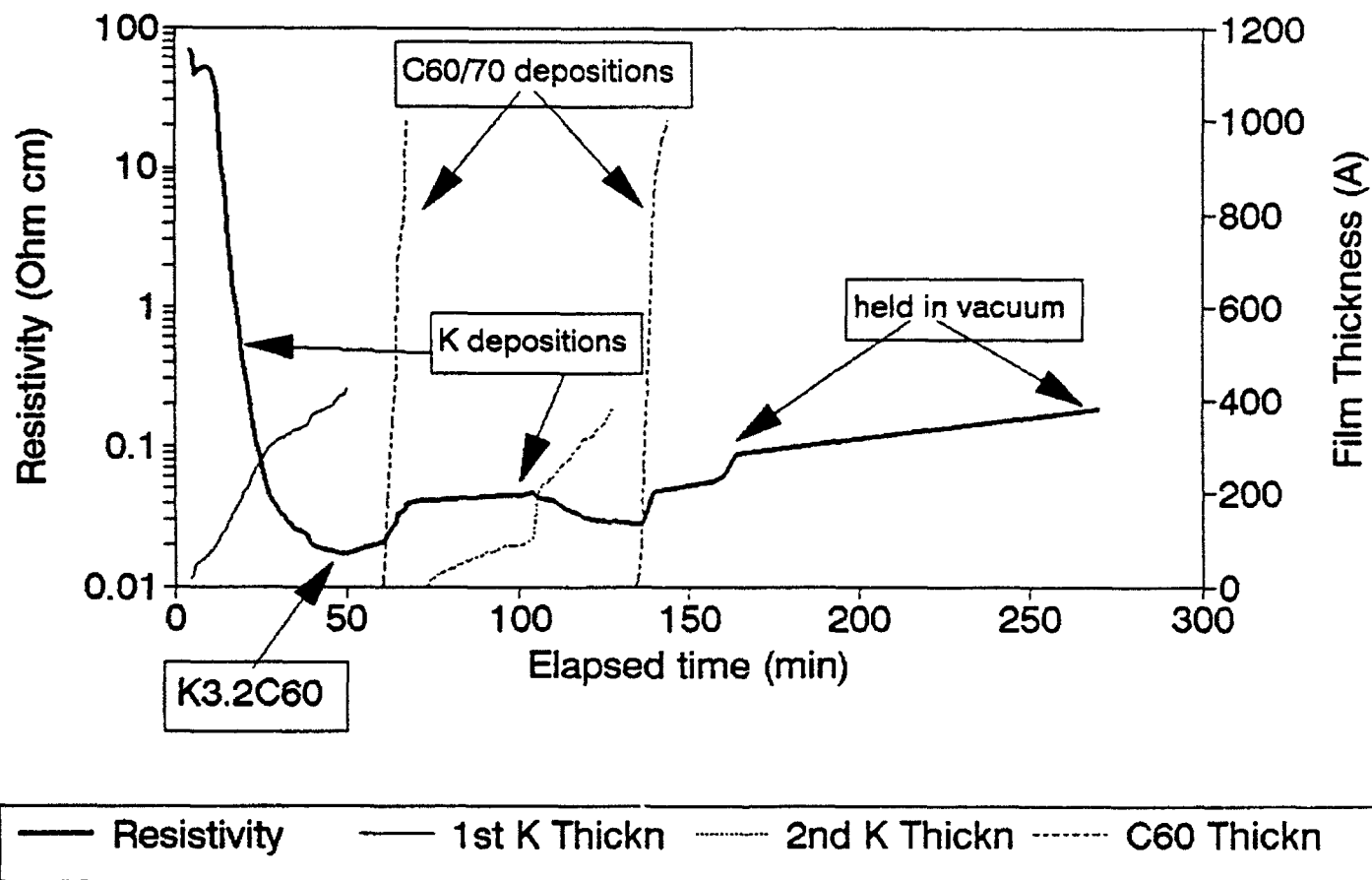


Figure 10. Test of Si as a protective overlayer for doped fullerenes films. Potassium thickness is nominal.

# C60 PROTECTIVE OVERLAYER

1000 Å C60/70, 3000 Å SiO, #079074

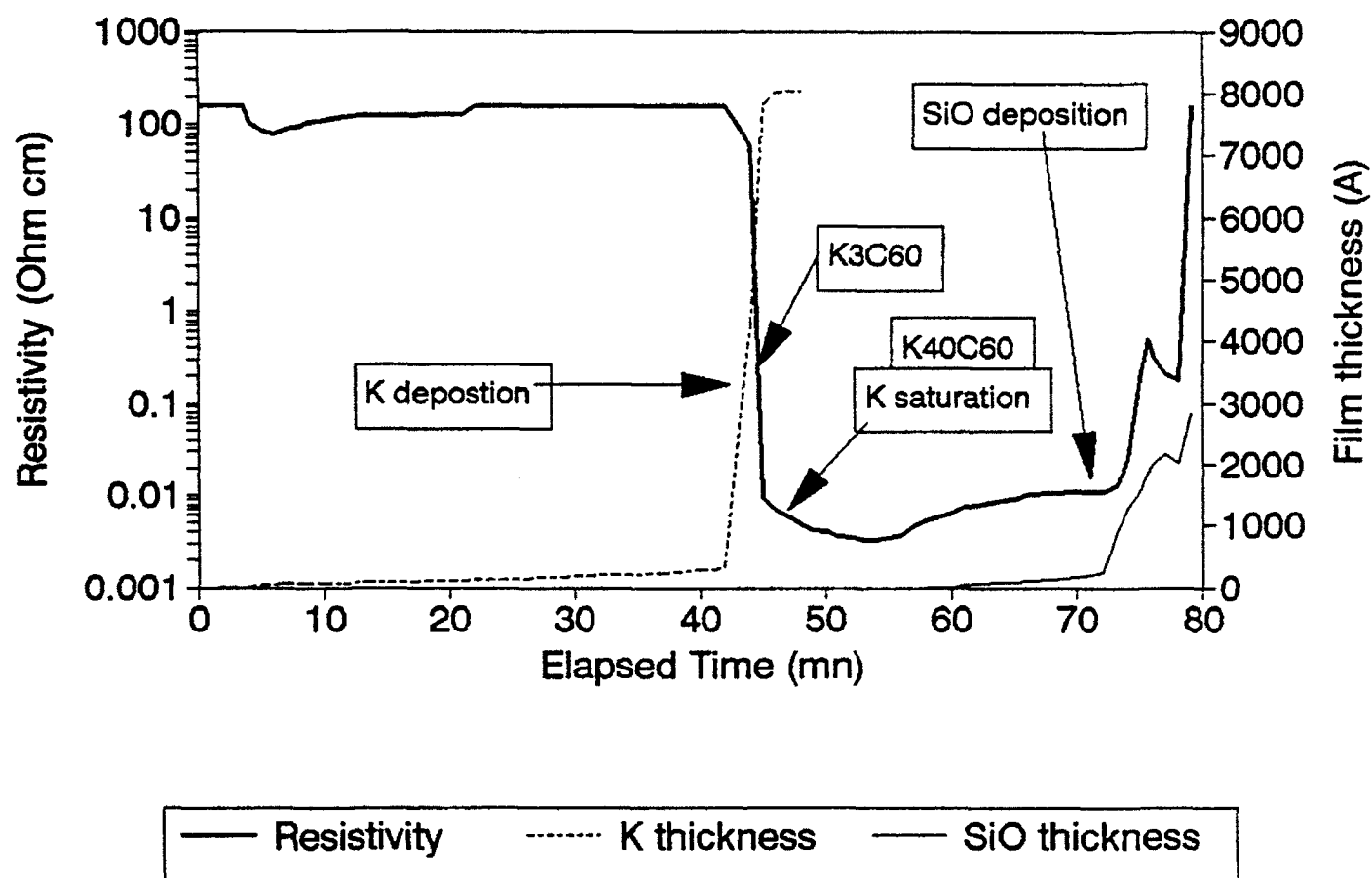


Figure 11. Test of SiO as a protective overlayer for doped fullerene films. Potassium thickness is nominal.

# K/C60 Superconductor CaF<sub>2</sub> Protective Film

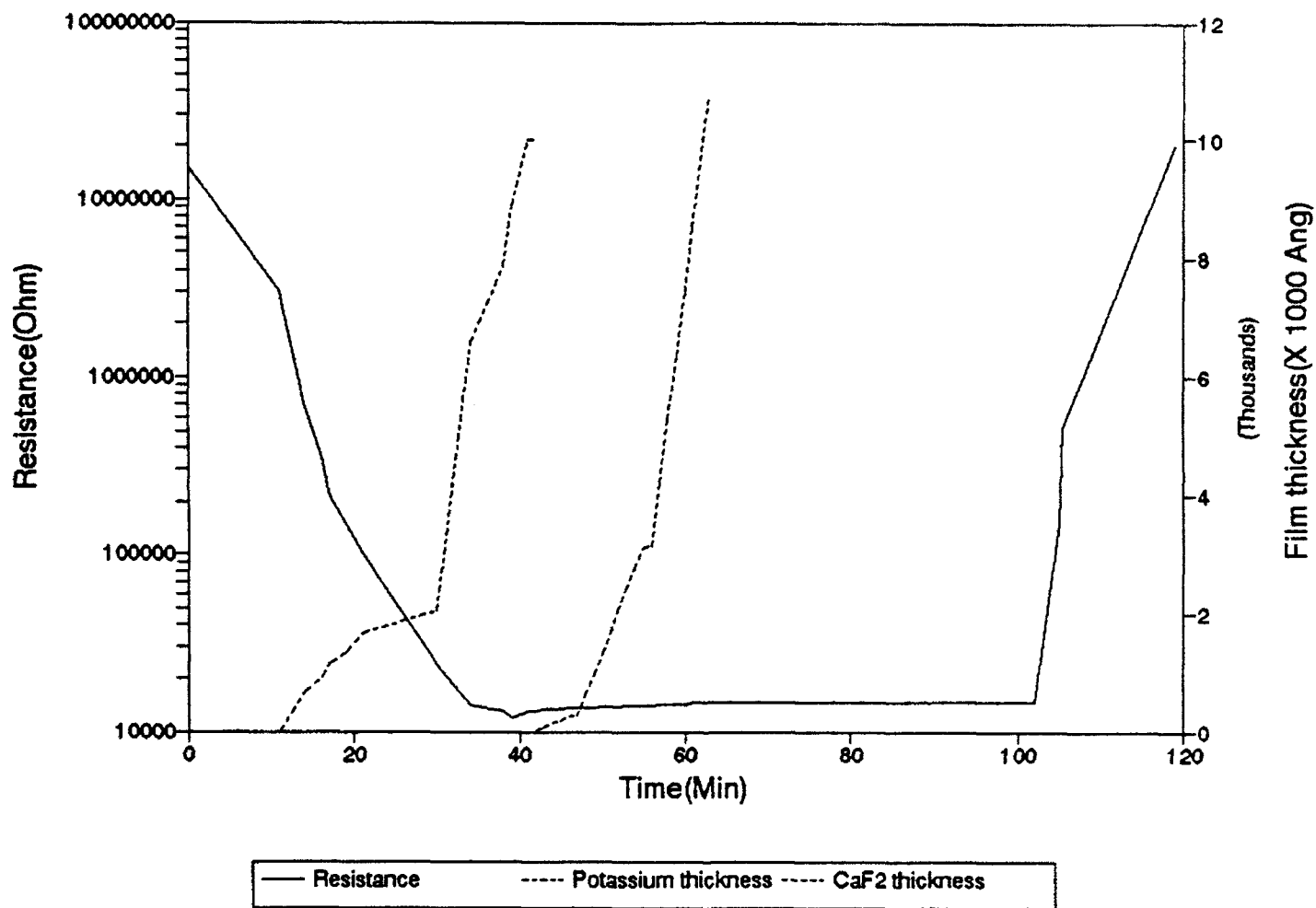


Figure 12. Test of CaF<sub>2</sub> as a protective overlayer for doped fullerene films. Potassium thickness is nominal.

# C60 PROTECTIVE OVERLAYER

2000A C60/70, 1  $\mu$ M POLYMER, #079096

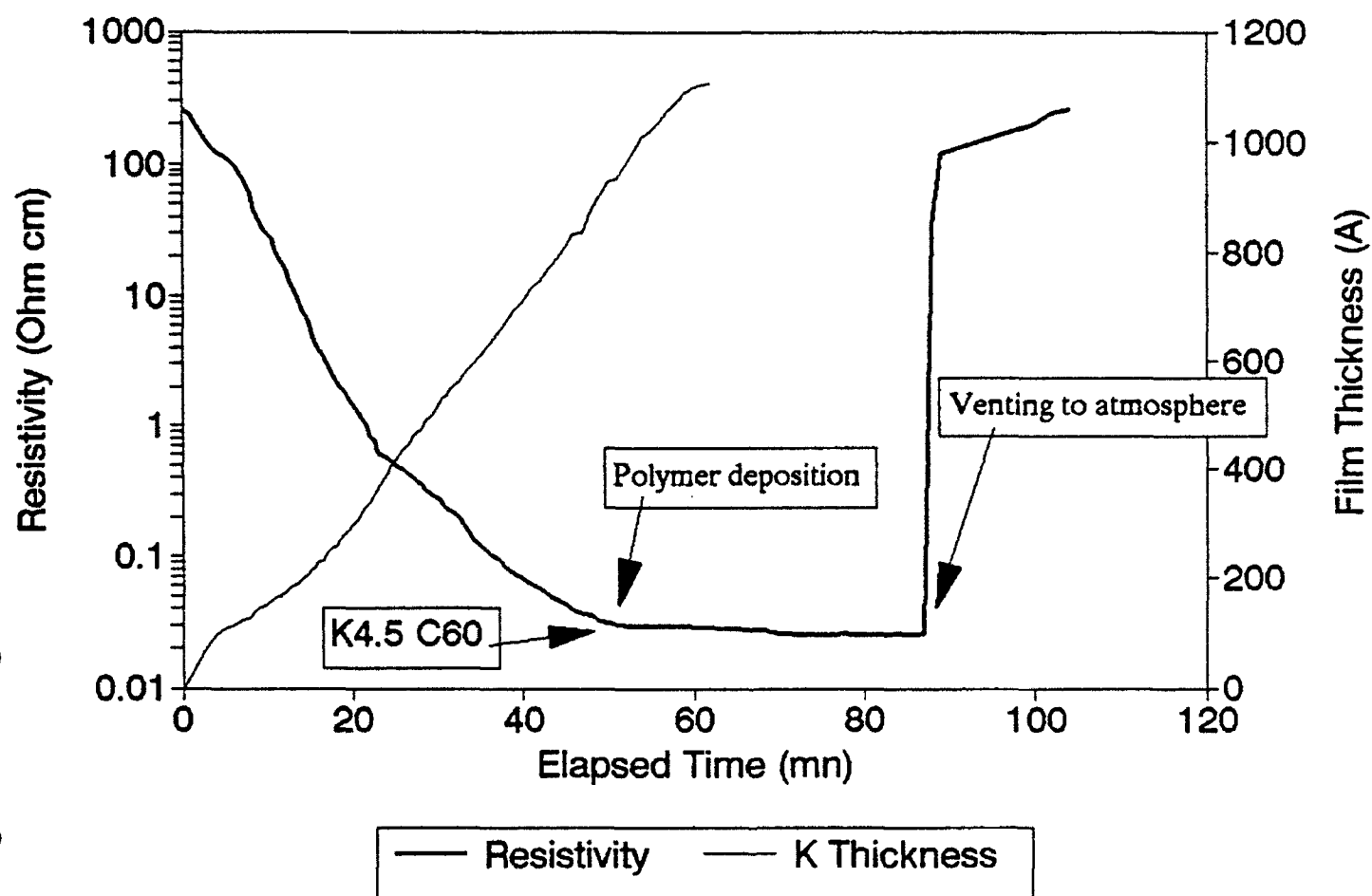


Figure 13. Test of polymer as a protective overlayer for doped fullerene films. Potassium thickness is nominal.

The resistance profile for an SiO deposition is shown in Figure 11. Again, for SiO the resistivity began to rise as soon as the SiO was deposited. The most plausible explanation is that SiO has an affinity for potassium that is stronger than that of the fullerenes. In any case, the resistivity rise matched the rate of deposition of the SiO until the point when air was let into the chamber. Air induced the resistance to rise to an unmeasurably high value since the SiO provided no protection.

The resistance profile for a CaF<sub>2</sub> deposition is shown in Figure 12. The CaF<sub>2</sub> did not react with the film in the evacuated chamber, but provided no protection since the resistance rose to an unmeasurably high value as soon as the chamber was vented.

The resistance profile for a polymer coating is shown in Figure 13. The polymer coating is produced by first depositing a monomer, and then curing the monomer with electron bombardment to polymerize it. The monomer and curing process caused no reaction in the resistance, and therefore did not react with the potassium. But the polymer did not provide any protection from the atmosphere since, as soon as the chamber was vented the resistance rose to an unmeasurably high value.

In general, the insulative overlayers provided little protection with the best protection provided by the Si coating. A summary of these depositions is presented in Table IV.

**Table IV.** Summary of Electrically Insulating Protective Overlayers

Protective Overlayer Composition	Fullerene Film Thickness	Overlayer Thickness	Protection Provided	Comments
Si	1 $\mu\text{m}$	0.55 $\mu\text{m}$	none	still saw some contamination from the air
SiO		0.3 $\mu\text{m}$	none	reacted with potassium
SiO <sub>2</sub>			none	did not adhere to fullerenes
CaF <sub>2</sub>			none	
polymer	0.2 $\mu\text{m}$	1 $\mu\text{m}$	none	

#### **4. Polymer/Aluminum Protective Multilayer**

A protection test was performed using the monomer/polymer deposition technique in combination with metallic overlayers. With the apparatus shown in Figure 2, up to three cycles of monomer deposition, monomer cure, and metal deposition were performed. Figure 14 shows the resistivity measured during the deposition of three polymer (5000 Å)/metal (500 Å) multilayers and subsequently during exposure to the atmosphere. As is indicated in Figure 14, the initial exposure to atmosphere a minimal or no change in resistivity and is the first evidence that the protective overlayer concept is feasible. In this sample, the role of the polymer is only to protect the sample from being shorted by the Al so the protection can be evaluated.

# C60 PROTECTIVE OVERLAYER

2000 A C60/70, #079097

3 x 5000 A POLYMER/Al COMPOSITE FILM

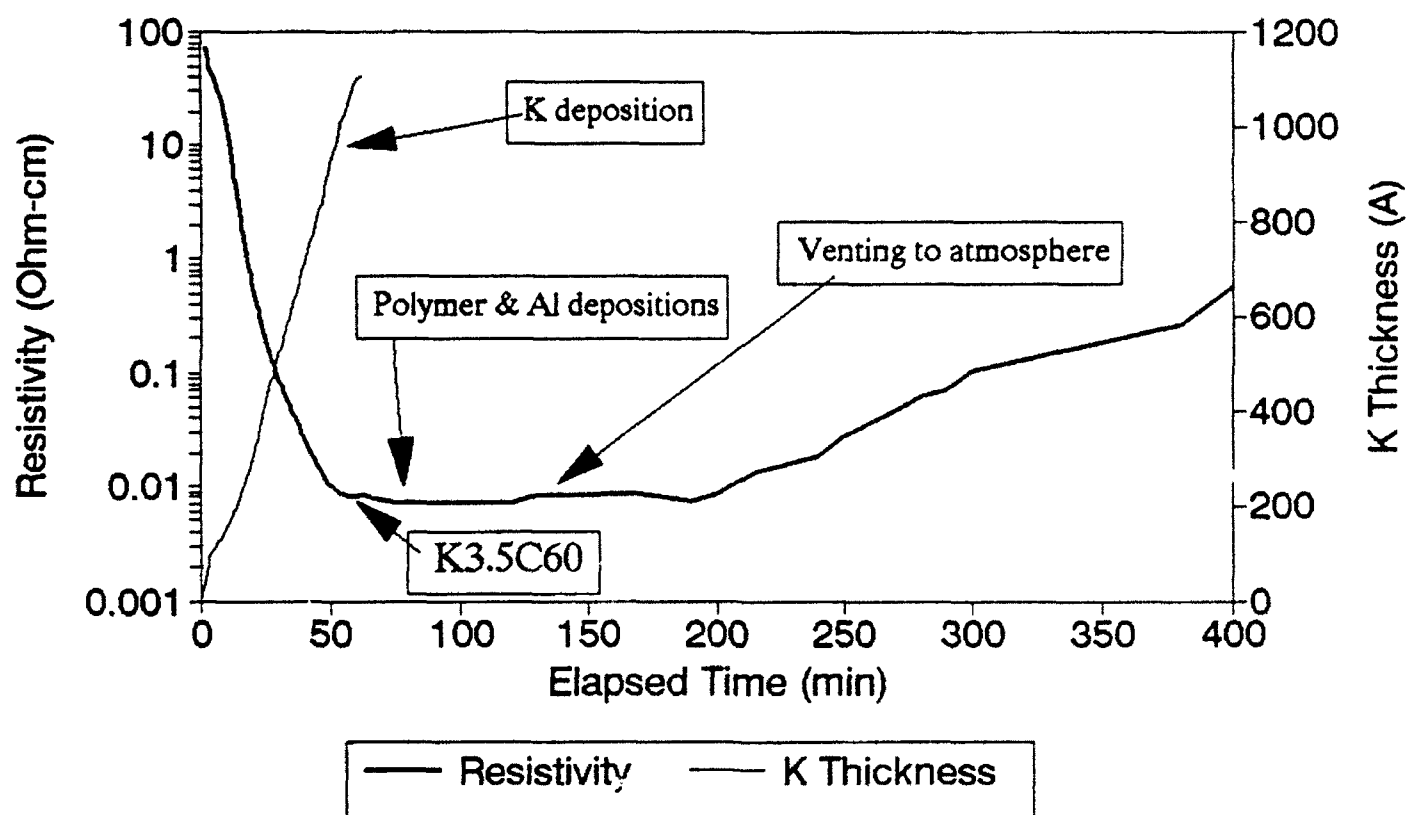


Figure 14. Resistivity record of polymer/Al multilayer deposition. Potassium thickness is nominal.

The conclusions drawn from this experiment were that metallic overlayers were a feasible method of protecting the doped fullerene samples, and that the Al thickness we used on the polymer/metal multilayer was too thin since the resistivity did start to rise when the sample had been exposed to the air for more than one hour. The rate of resistivity rise indicated that with 500 Å metal layers, roughly half the potassium is oxidized after three hours. Therefore metal protective layers should be somewhat thicker.

## 5. Metallic Protective Layers

Potassium doped fullerene films had overlayers of Cu, Ag, and Al deposited over the face of the film. These metals were chosen because available evidence indicated little or no alloying potential with potassium. Binary phase diagrams of potassium are difficult to come by presumably because of its reactivity. Of the three chosen, aluminum was emphasized in the experiments because, although it is very reactive with oxygen, it is known for protecting itself from oxygen attack. Samples were prepared with a single thickness of Ag and Cu. Aluminum was deposited to several thicknesses. In addition, several samples were included in the 5000 Å Al deposition. These were arrayed across the substrate plane so that they received slightly varying thicknesses of fullerenes, potassium, and aluminum.

The resistivity of the samples was recorded during the depositions. For the multiple samples of the 5000 Å Al deposition, the resistivity of one sample was recorded. The resistivity records of the 5000 Å, 2000 Å, 1000 Å, and 600 Å Al, the Cu, and the Ag overlayers are shown in Figures 15 to 20 respectively. As is expected, the resistivity is

# C60 PROTECTIVE OVERLAYER

2000 Å C60/70, 5000 Å Al, #079091

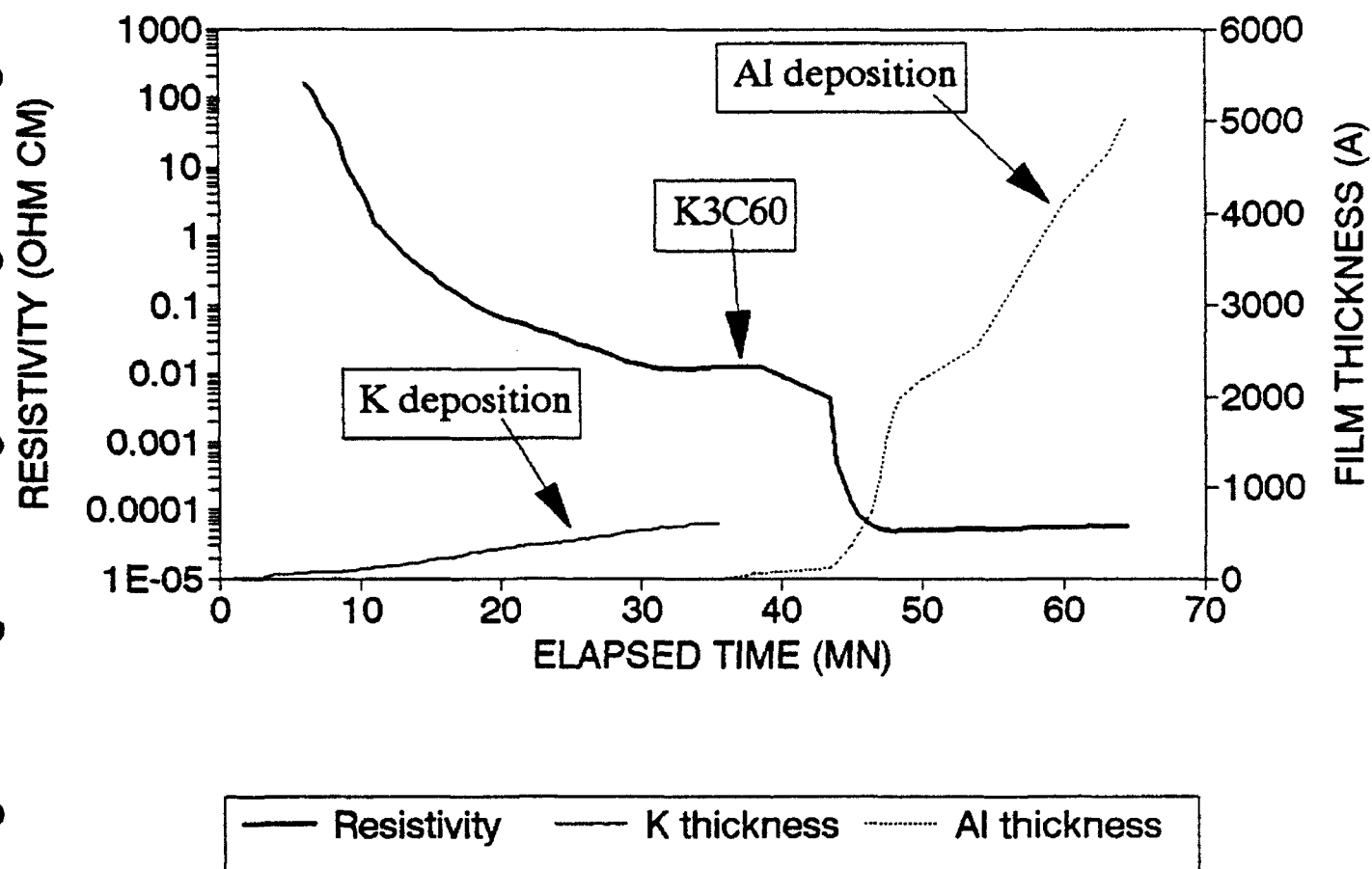


Figure 15. Resistivity record of 5000 Å overlayer deposition. Potassium thickness is nominal.

# C60 PROTECTIVE OVERLAYER

2000 Å C60/70, 2000 Å Al, #079087

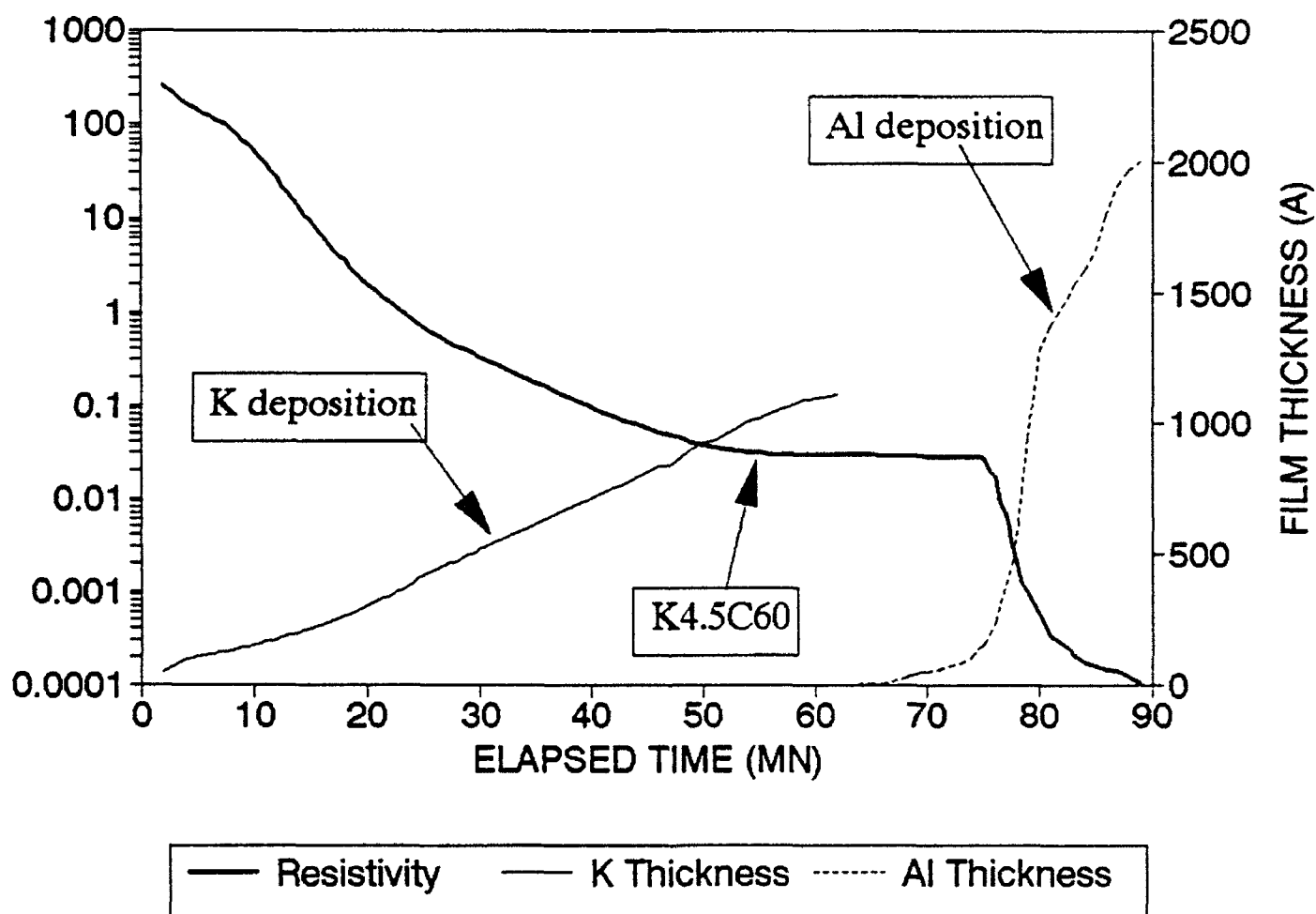


Figure 16. Resistivity record of 2000 Å Al overlayer deposition. Potassium thickness is nominal.

# C60 PROTECTIVE OVERLAYER

4500 Å C60/70, 1000 Å AL, #079085

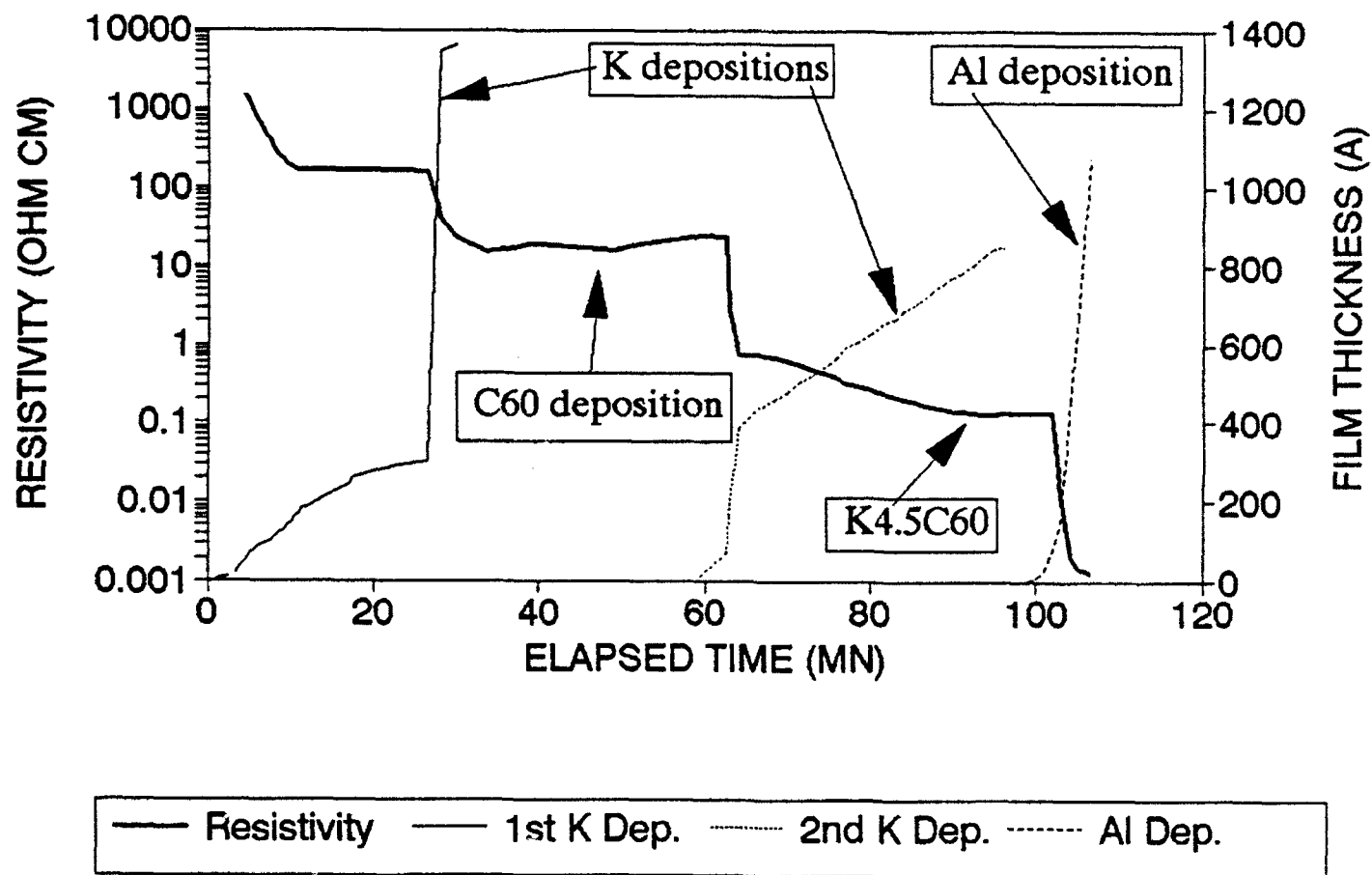


Figure 17. Resistivity record of 1000 Å Al overlayer deposition. Potassium thickness is nominal.

# C60 PROTECTIVE OVERLAYER

2000 Å C60/70, 600 Å Al, #079083

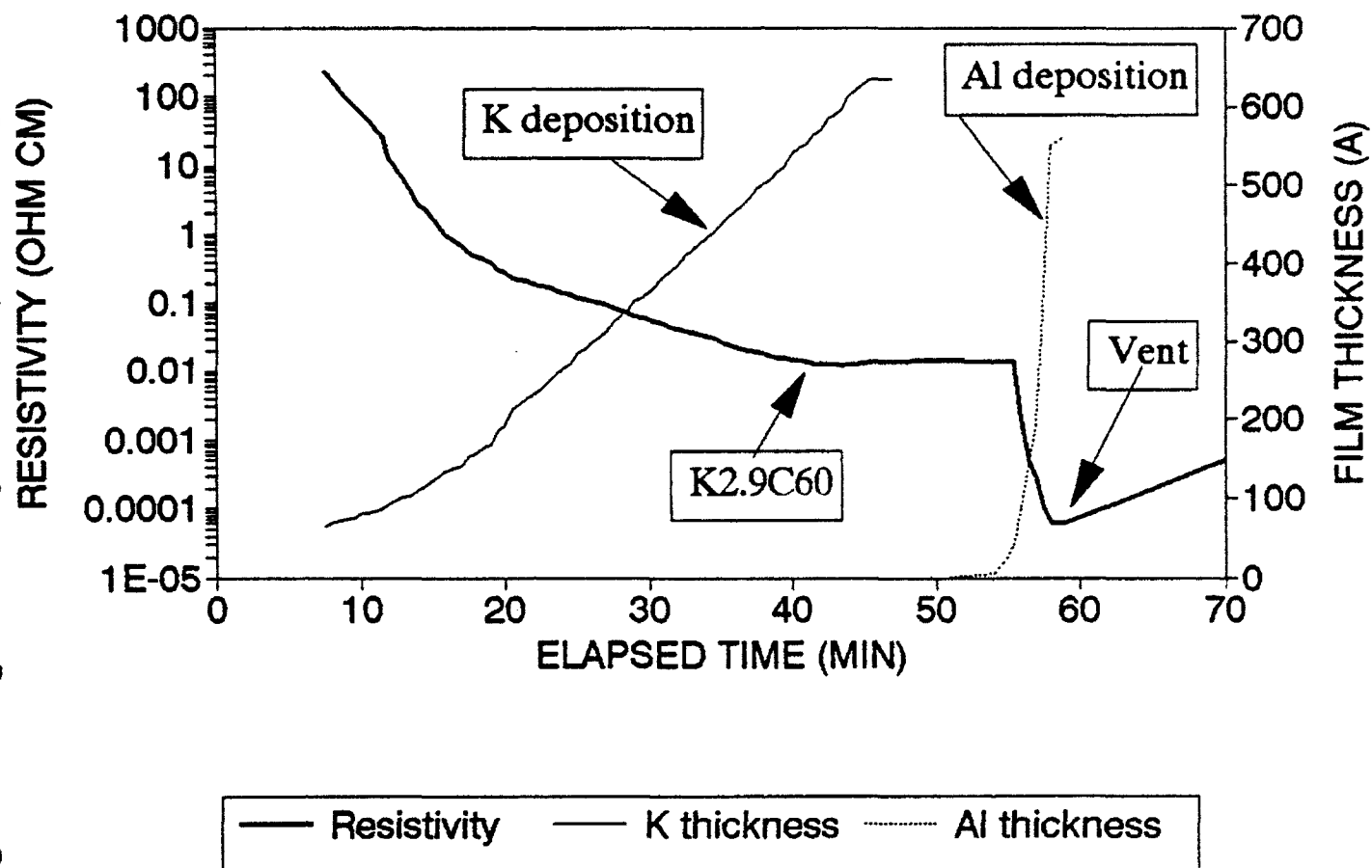


Figure 18. Resistivity record of 600 Å Al overlayer deposition. Potassium thickness is nominal.

# C60 PROTECTIVE OVERLAYER

2200 A C60/70, 1  $\mu$ M Cu, #079105

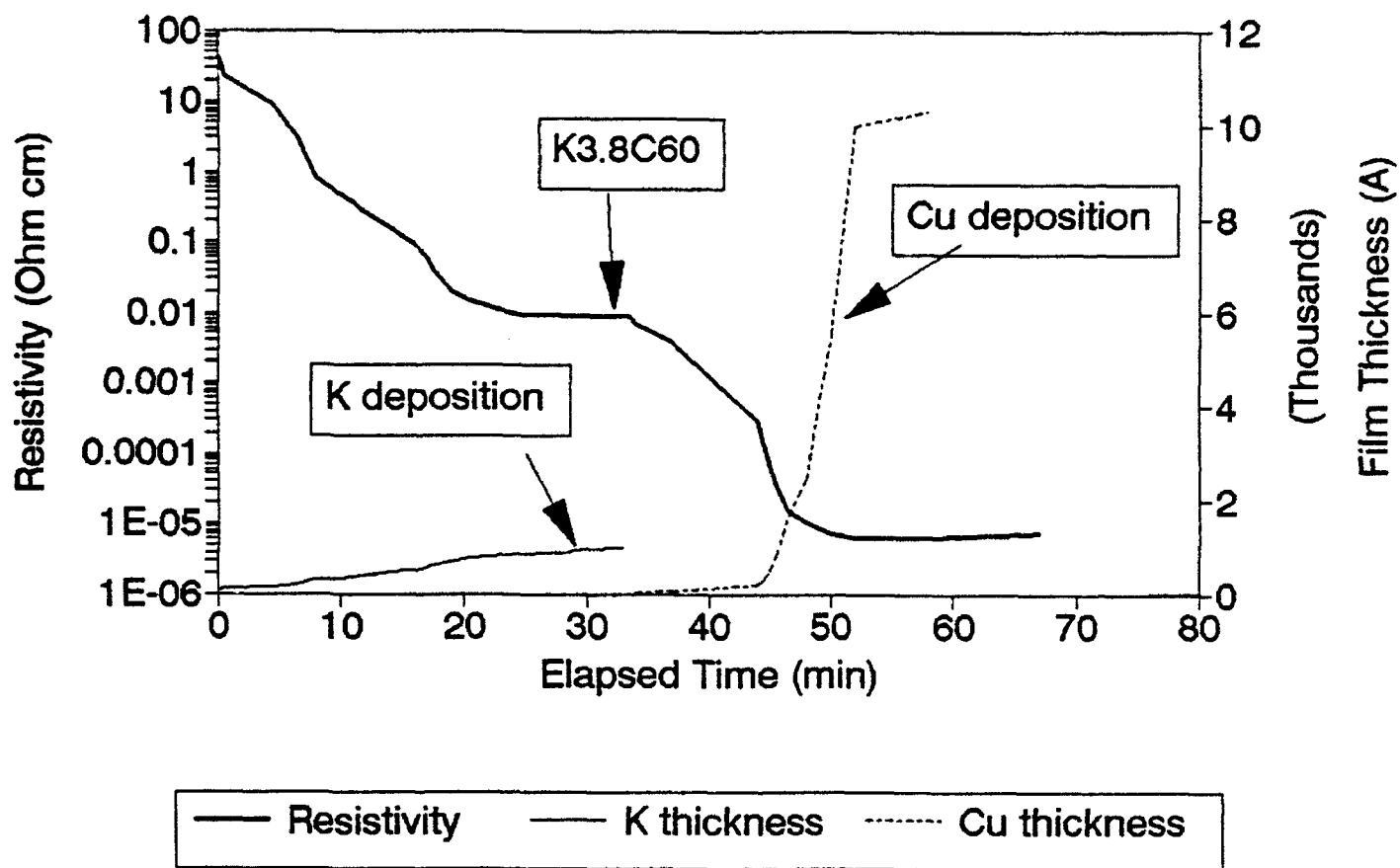


Figure 19. Resistivity record of CU overlayer deposition. Potassium thickness is nominal.

# C60 PROTECTIVE OVERLAYER

2100 A C60/70, 1  $\mu$ M Ag, #079107

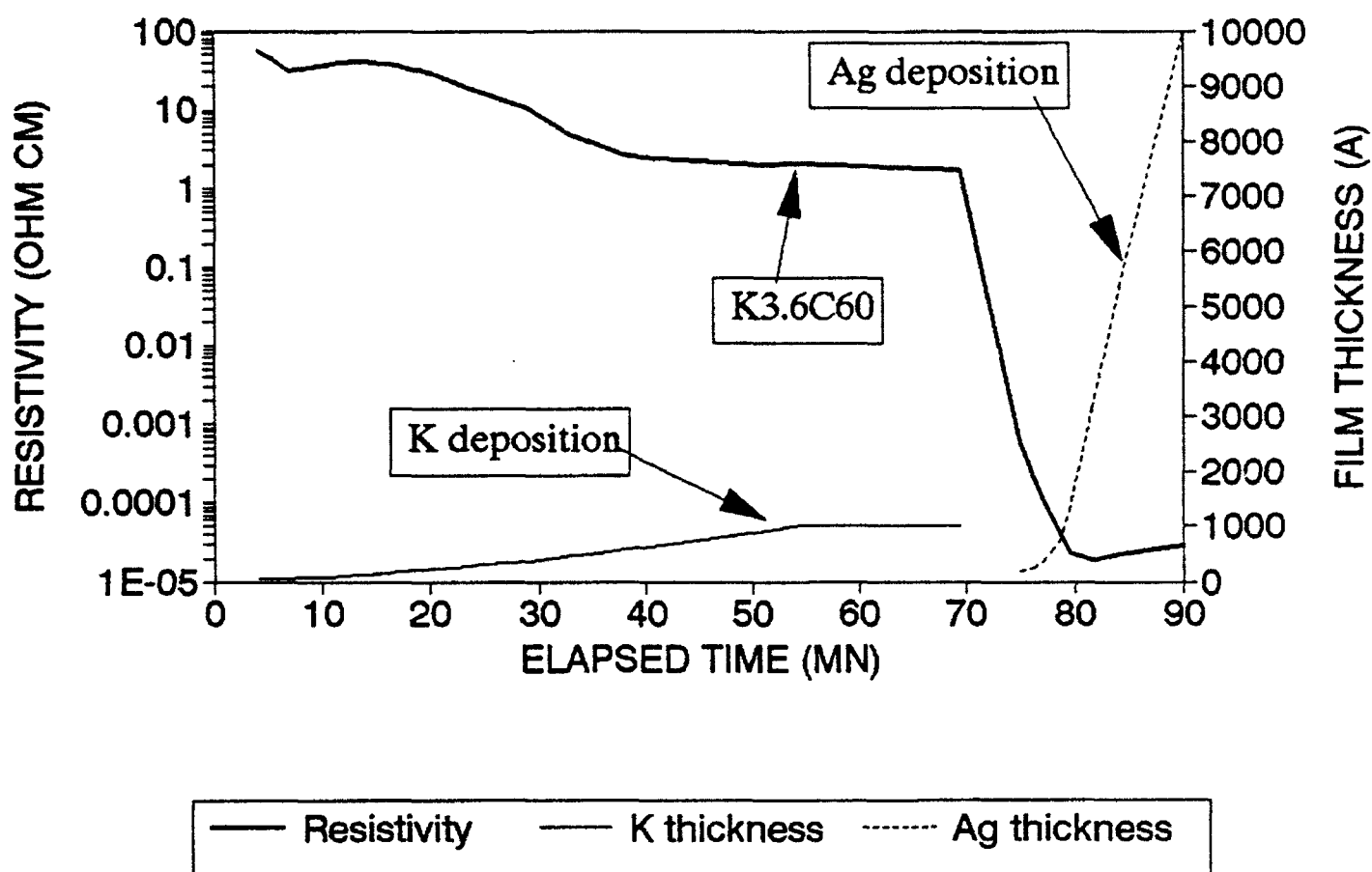


Figure 20. Resistivity record of Ag overlayer deposition. Potassium thickness is nominal.

minimized by a potassium deposition and when the metallic overlayer is deposited, the resistivity drops. Some of the metal layers are so thick that the resistance reaches a minimum and saturates as the metal layer becomes thicker. The saturation is a manifestation of our simple two probe measurement technique rather than a measure of the intrinsic resistivity of the metal overlayer.

For the most part, the resistance of the sample did not change as the chamber was vented and is not shown in the figures. The exception is the sample with a 600 Å Al layer shown in Figure 18.

To test samples with metallic overlayers for protective ability they were sent to Ames for cryogenic resistivity measurements. The resistivity ratios resulting from that measurement and deposition thicknesses are shown in Table IV. None of the samples showed superconductivity as indicated by nonlinear I-V characteristics. Samples were all measured with currents of 1 and 10 milliamps. The sample with the 2000 Å Al coating was measured with currents down to 10  $\mu$ A and demonstrated a linear I-V characteristic. The lack of superconductivity may be due to permeation of oxygen through or around the protective barriers, but since aluminum is such an effective oxygen barrier, the lack of superconductivity is more likely to be due to impurities absorbed during the doping process. If this is the case then a more definitive test is required with samples made in a UHV vacuum system. Although there was no super conductivity observed, the high resistivities during deposition indicate that the impurities are incorporated during the film depositions.

The results from the polymer/metal multilayer sample suggest that Al metal will indeed protect from oxidation if it is thick enough.

Table IV. Deposition thicknesses and cryogenic resistivity ratios for metallic overlayers.

Protective Overlayer		Fullerene Thickness (Å)	Resistance Ratios	
Material	Thickness (Å)		$R_{rt}/R_{LN2}$	$R_{rt}/R_{LN2}$
Al	5000 - #1	2000	1.8	2.2
Al	5000 - #2	2000	2.5	3.0
Al	5000 - #3	2000	2.7	3.4
Al	5000 - #4	2000	3.0	3.9
Al	2000	2000	2.5	3.0
Al	1000	4500	2.4	3.7
Al	600	2000	*	*
Cu	10000	2200	**	**
Ag	10000	2100	1.6	1.9

\* Electrical solder contact broken during cryogenic measurement, unrepairable.

\*\* Film cracked during cryogenic cooldown.

## 6. Nickel Tube Protection

The initial test at Ames on the Ni protected wire made at MER indicated no superconductivity (critical current  $< 1 \text{ A/cm}^2$ ). However this result is from the first (and only) Ni protected wire produced. It is probable that with refinement of the doping technique inside a sealed nickel tube superconducting fullerene wires could be produced.

### B. In-cage Dopants

Three metals were used as in-cage dopants, La, Sr, and Ag. These metals were incorporated into graphite rods and prepared as previously described with toluene and NMP extracted solids as products. These solids were tested with EDS for the presence of the dopant metals. The results of the EDS test are tabulated in Table V.

As discussed previously, toluene is used to extract the fullerene allotropies  $C_{60}$ ,  $C_{70}$ , and  $C_{84}$ , the most stable and spherical of the fullerenes. NMP dissolves much of the soot produced in the arc, but does not dissolve graphite powder formed with conventional methods. As is indicated by the EDS test results, none of the toluene extracted material showed any metal using the EDS detection methods implying that  $C_{60}$ ,  $C_{70}$ , and  $C_{84}$ , at least did not accept in-cage metal dopants, or if they did accept in-cage dopants, the doped fullerenes were not toluene soluble. The more complicated solutes in NMP did show some encapsulation, or at least some binding of the metal dopants. These samples were tested at Ames for superconductivity.

**Table V.** EDS test of solid products for metal dopants. Yes means metal was detected in the extract.

Doping Composition	Solvent used to extract solid product	
	toluene	NMP
$\text{Ag}_1\text{C}_{60}$	no	yes
$\text{Sr}_1\text{C}_{60}$	no	no
$\text{Sr}_5\text{C}_{60}$	no	no
$\text{Hf}_5\text{C}_{60}$	no	no
$\text{La}_1\text{C}_{60}$	no	yes
$\text{La}_5\text{C}_{60}$	no	yes

The samples extracted from NMP which contained metals were tested to determine if magnetic separation was a feasible approach. The samples were diluted until they were nearly transparent, stirred, placed near a strong permanent magnet, and allowed to settle overnight. Some material precipitated, mostly toward the bottom but there was a small anisotropy in the distribution of material with more collecting on the side by the magnet. This anisotropy was not large enough to be pursued as a separation technique given the limitations of a Phase I SBIR program.

Figure 21 shows the magnetization data of the sample extracted from  $\text{Ag}_1\text{C}_{60}$  soot using NMP. Figure 21a indicates that the overall signal is diamagnetic. Additionally there is a low level flux exclusion (difference between zfc and fc curves) that is not necessarily associated with the diamagnetism. If that signal were due to a superconducting phase, it would indicate that the volume of superconducting material would be on the order of 0.01% of the total sample volume. However, there is still a definite magnetic flux exclusion transition detectable above the level of the noise. That transition occurs at approximately 40K. The flux exclusion maybe caused by either superconductivity or ferromagnetism. These possibilities are discussed in detail below with the  $\text{Th}_{0.75}\text{C}_{60}$  sample which had a stronger signal and was therefore easier to test.

The magnetization as a function of field shown in Figure 21b shows a paramagnetic signal. This curve suggests that there are two paramagnetic phases, the high susceptibility phase dominates the signal at low fields, but then saturates at approximately 1000 Oe, while at higher fields there is a lower susceptibility. This interesting feature crops up several times throughout the course of this investigation. The change in slope of the M vs. H curve can be attributed to the saturation of some magnetic component of the metal/fullerene complex. At this point we are not able to tell whether the saturating moments are magnetic dipoles on the metal atoms or whether they are circulating currents on the fullerene molecules. The saturating moments are generally associated with the existence of flux exclusion. However, as will be shown later, the saturation of the magnetization occurs at temperatures above the transition temperature indicating that the flux exclusion is not specifically associated with the saturating magnetic moments.

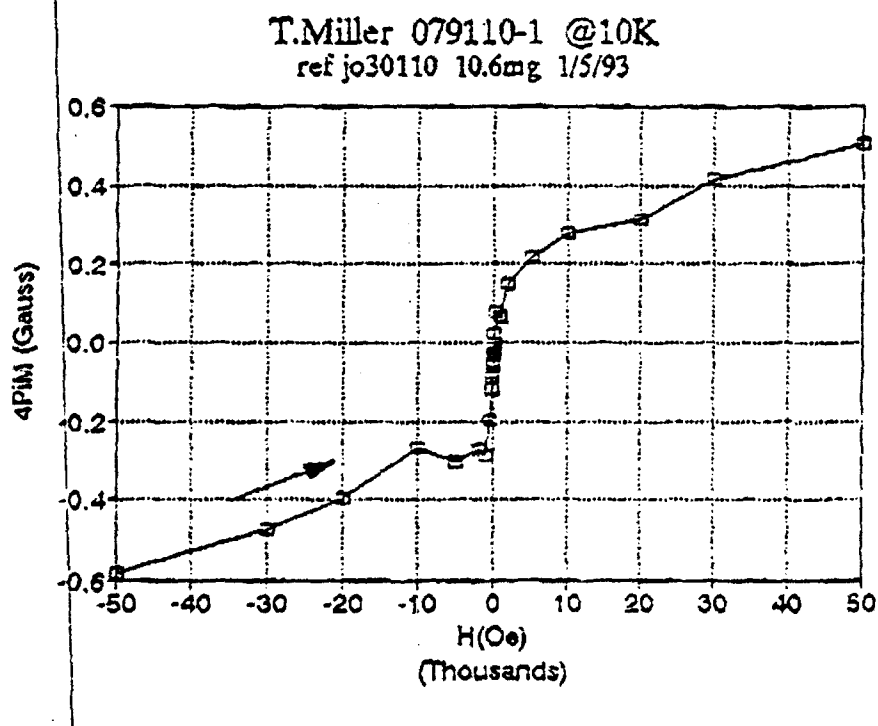
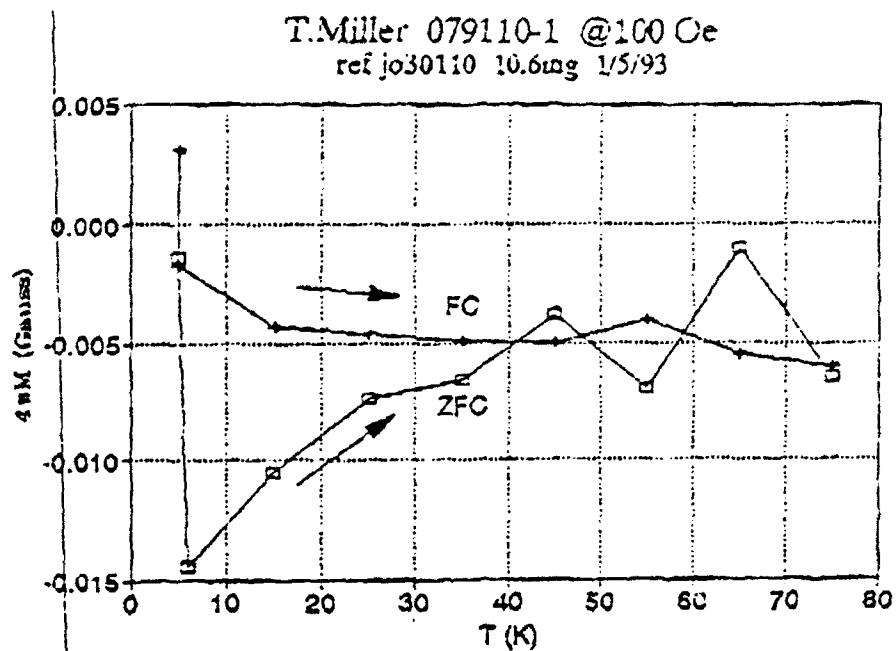


Figure 21. Magnetization of arc burned  $\text{Ag}_1\text{C}_{60}$  sample as a function of a) temperature using a 100 Oe field, and b) as a function of field at 10 K.

The combination of flux exclusion and magnetic saturation indicates an active magnetic or superconducting feature to these compounds. Experiments that will absolutely confirm the superconductivity remain to be performed. For now we can only conclude that if it is a superconductivity phenomena, then samples that show a stronger flux exclusion are closer to the pure superconducting phase.

Figure 22 shows the magnetization data of the sample extracted from  $\text{La}_1\text{C}_{60}$  soot using NMP. It is difficult to determine whether the overall magnetization is diamagnetic or paramagnetic since the signal is small enough to generate significant scatter. There is a trend in this data suggesting that there is still some flux exclusion to a lesser extent than the previous example, again with a transition temperature of approximately 40 K. Figure 22b shows a similar paramagnetic feature to the previous silver doped sample, but because the high field susceptibility is stronger, the transition from high susceptibility at low fields to a lower susceptibility at high fields is less noticeable. Since both the flux exclusion and magnetic saturation are weaker in  $\text{La}_1\text{C}_{60}$ , any associated superconductivity is also weaker.

Figure 23 shows the magnetization data of the sample extracted from  $\text{La}_5\text{C}_{60}$  soot using NMP. Overall the signal is diamagnetic with little separation between the zfc and fc curves. This sample has a higher susceptibility at high fields than the previous two. It also shows less (if any at all) of the low field transition from high to low susceptibility. Since both the flux exclusion and magnetic saturation are weaker in  $\text{La}_5\text{C}_{60}$  than  $\text{La}_1\text{C}_{60}$  or  $\text{Ag}_1\text{C}_{60}$ , any associated superconductivity is also weaker.

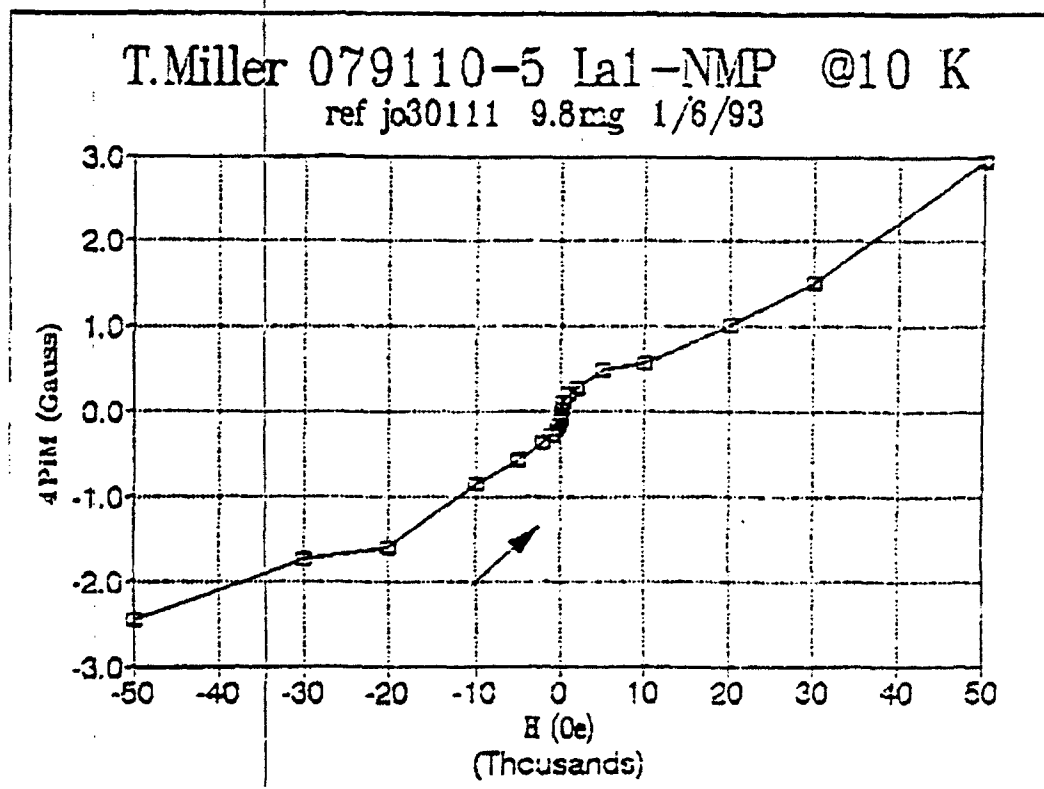
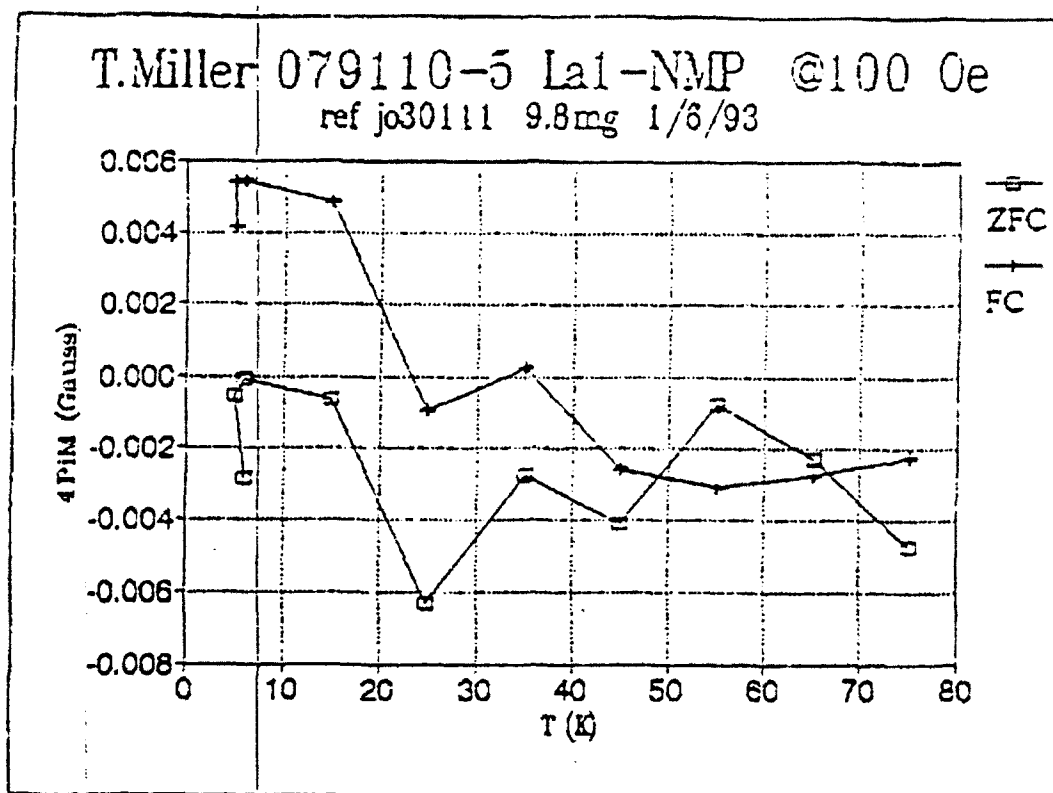


Figure 22. Magnetization of arc burned La<sub>1</sub>C<sub>60</sub> sample as a function of a) temperature using a 100 Oe field, and b) as a function of field at 10K.

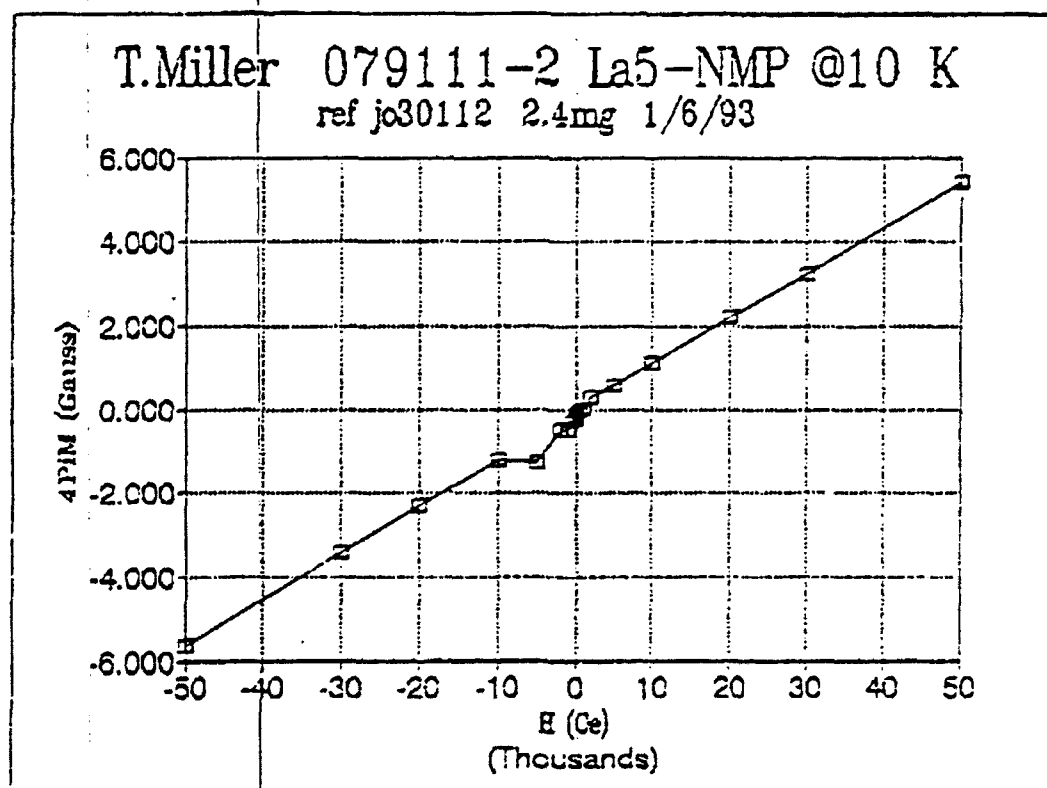
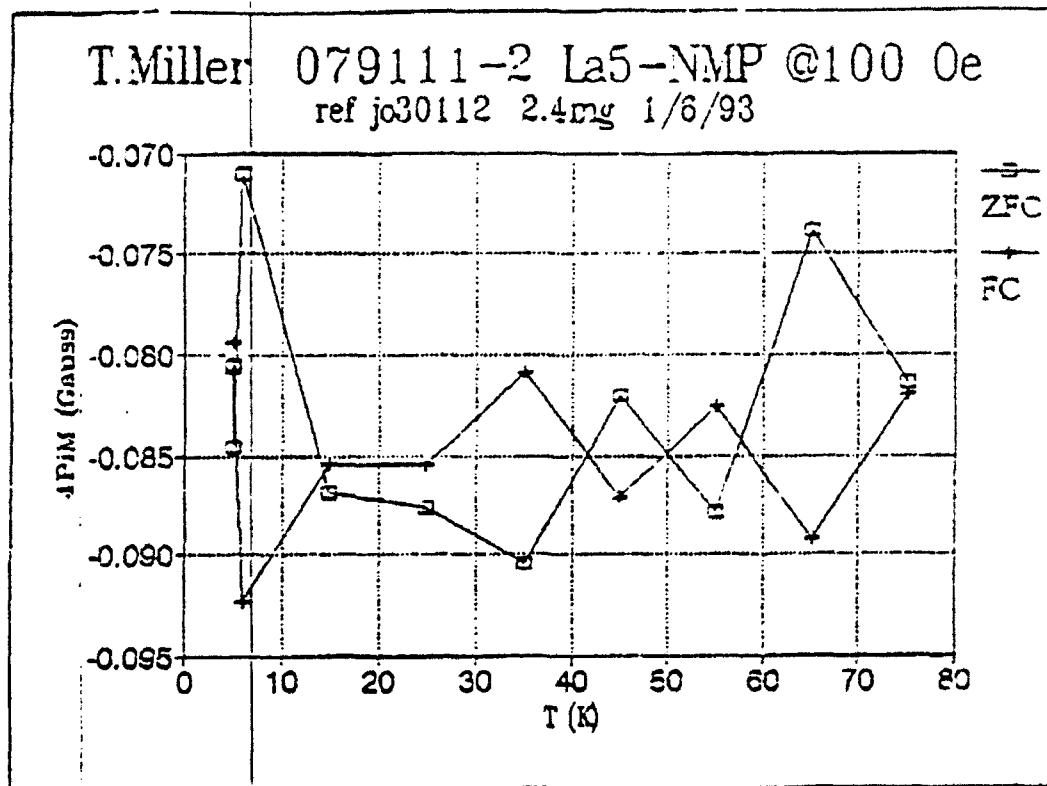


Figure 23. Magnetization of arc burned La<sub>5</sub>C<sub>60</sub> sample as a function of a) temperature using a 100 Oe field, and b) as a function of field at 10K.

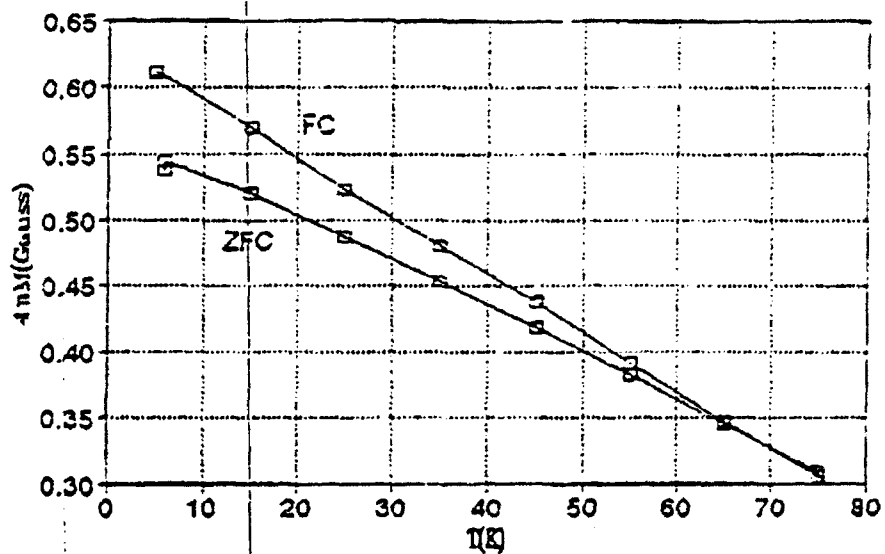
### C. Alternate Dopants

Due to the failure of most of the nickel tubes treated in the HIP experiment, only the Zn doped sample and the Th doped samples (which were treated separately) were tested in the magnetometer at Ames. The results showed flux expulsion (a separation of the zfc and fc magnetization) in several cases. Because the overall signal was paramagnetic and the percentage of flux expulsion was small, the flux expulsion would be attributed to a small volume percent of superconducting material or a ferro- or ferri- magnetic material.

Because the signals were small the quartz sample holder was refined to eliminate any systematic errors from the quartz itself (quartz has a small diamagnetic signal). The first holders used were small quartz tubes with a quartz plug in the middle to hold the sample. That constriction generates a signal that is spatially separated from the sample and leads to errors in small sample signals. The quartz plug holder was replaced by a solid quartz holder with a gap in the middle for the sample. The gap does have a negative quartz signal, but that signal directly overlays the sample signal and does not distort the spatially dependent magnetization signal. Calibrated signals from quartz gaps are then subtracted from the overall signal. The magnetization data discussed below specifies the type of holder used for each case, either quartz plug or quartz gap.

The magnetization data for the HIPed  $\text{Zn}_6\text{C}_{60}$  sample in an quartz plug holder is shown in Figure 24. There is a strong temperature dependence and diamagnetic signal that turned out to be due to an impurity in that particular sample holder. When we transferred

T.Miller 079104-12 ZN6:Cl @100 Oe  
ref jc30109 21.8mg 1/5/93



T.Miller 079104-12 Zn6:Cl @10K  
ref jc30109 21.8mg 1/5/93

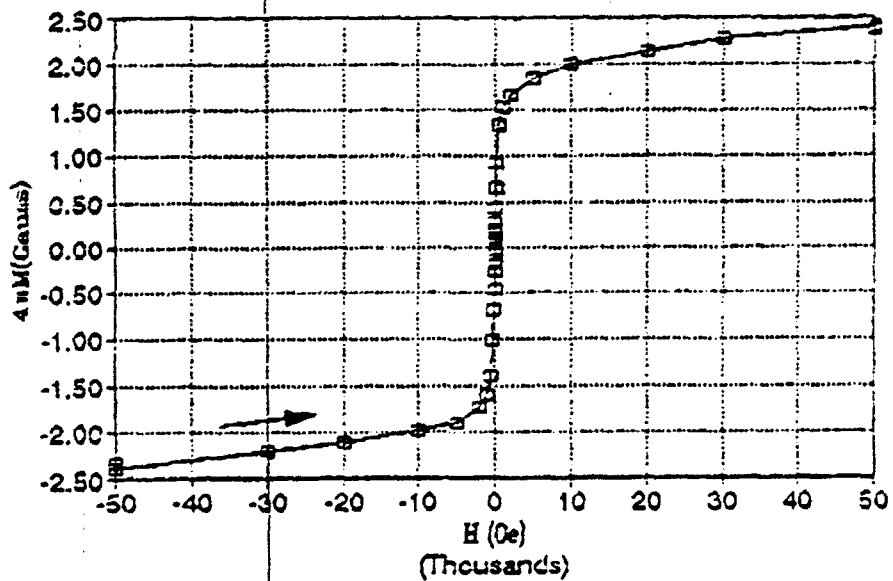


Figure 24. Magnetization of HIPed  $\text{Zn}_6\text{C}_{60}$  sample as a function of temperature in a quartz plug holder.

the sample to a quartz gap holder we recorded the data in Figure 25. The temperature dependence is gone and the magnitude of the signal is much smaller. The discrepancy between the quartz gap and the quartz plug holder has to do with the positioning of that particular sample with relation to the quartz plug, or an impurity in that specific quartz plug. That magnitude of discrepancy between quartz plug and quartz gap holder was a singular exception to the rule, as will be seen below. When measured in the well-controlled quartz gap holder, Figure 25 shows little evidence of a superconducting transition in the HIPed  $\text{Zn}_6\text{C}_{60}$  sample.

The magnetization data from the three thorium doped samples,  $\text{Th}_{0.75}\text{C}_{60}$ ,  $\text{Th}_{1.5}\text{C}_{60}$ , and  $\text{Th}_3\text{C}_{60}$ , in the quartz plug holders are plotted in Figures 26, 27, and 28 respectively. Unfortunately, by examining the data it appears as though there was some mixup in the samples. According to our records the samples are as labeled here. But if the graphs are reorganized in the order  $\text{Th}_{0.75}\text{C}_{60}$ ,  $\text{Th}_3\text{C}_{60}$ ,  $\text{Th}_{1.5}\text{C}_{60}$  there is a clear trend both in the apparent flux expulsion and in the magnitude of the magnetization. That trend is toward a stronger paramagnetic signal as the flux exclusion gets stronger. This fact points toward a ferro- or ferri- magnetic material but does not exclude the possibility of a small portion of the material becoming more superconducting, while the remaining material becomes more paramagnetic. In any case, the following discussion is geared primarily toward the sample marked  $\text{Th}_{0.75}\text{C}_{60}$  and not toward a comparison between the samples.

T.Miller 079104-12 6Zn @10K  
ref jo30123 5.3mg 1/14/93

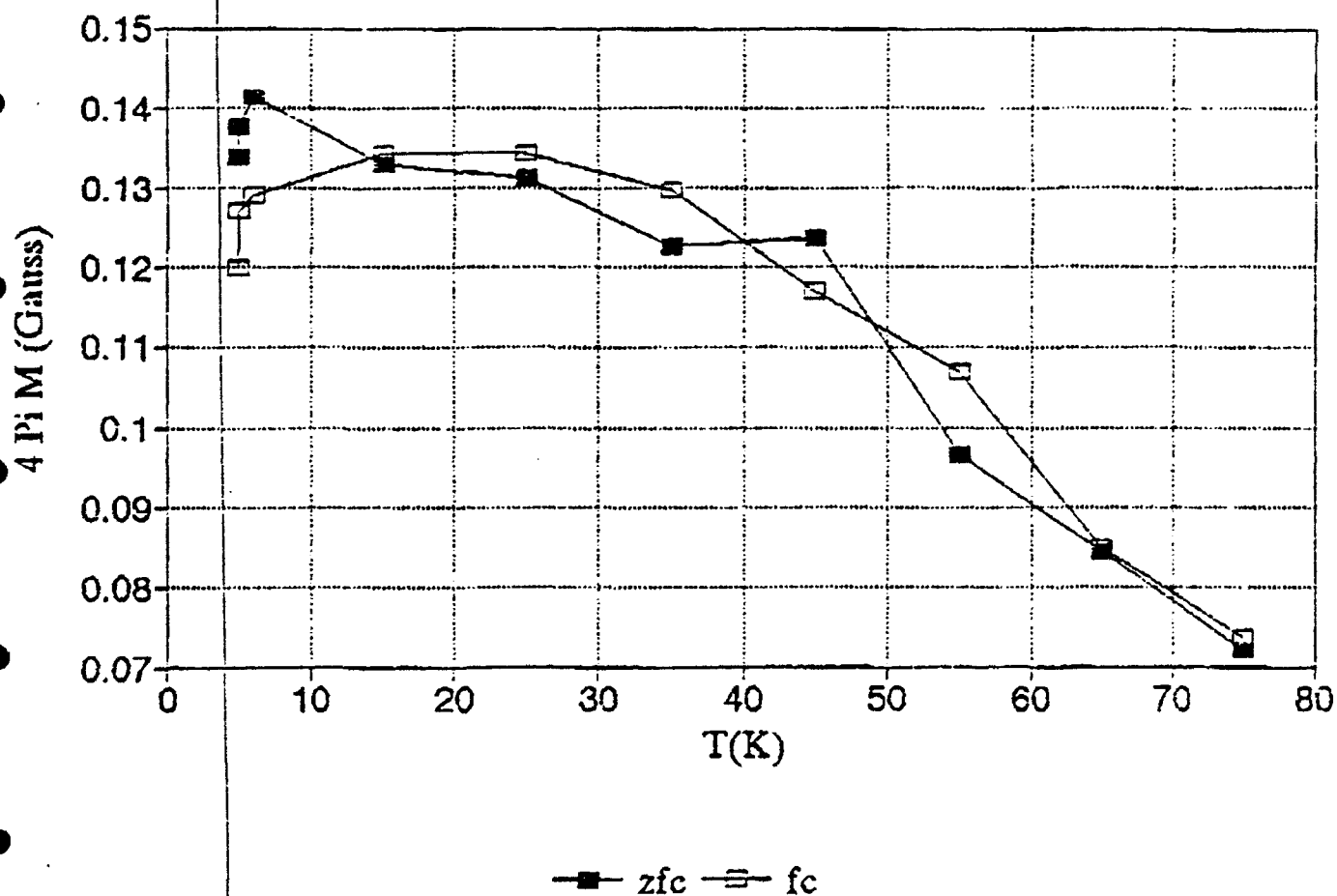


Figure 25. Magnetization of HIPed  $\text{Zn}_6\text{C}_{60}$  sample as a function of temperature in a quartz gap holder.

T.Miller ThC60 #9 Batch#3 @50 Oe  
 ref jo3059 6.4mg. 11/11/92

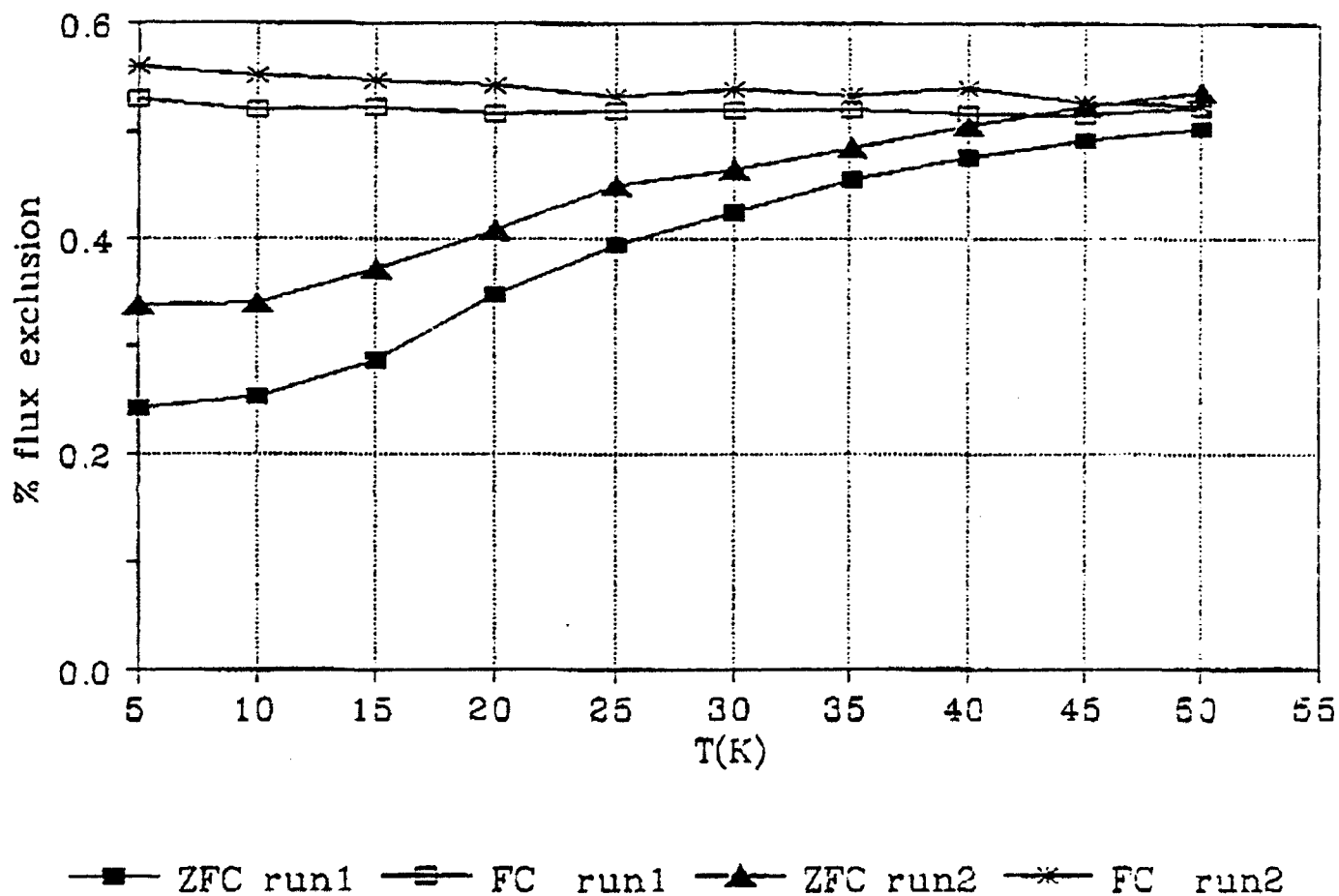


Figure 26. Magnetization of heat treated  $\text{Th}_{0.75}\text{C}_{60}$  as a function of temperature.

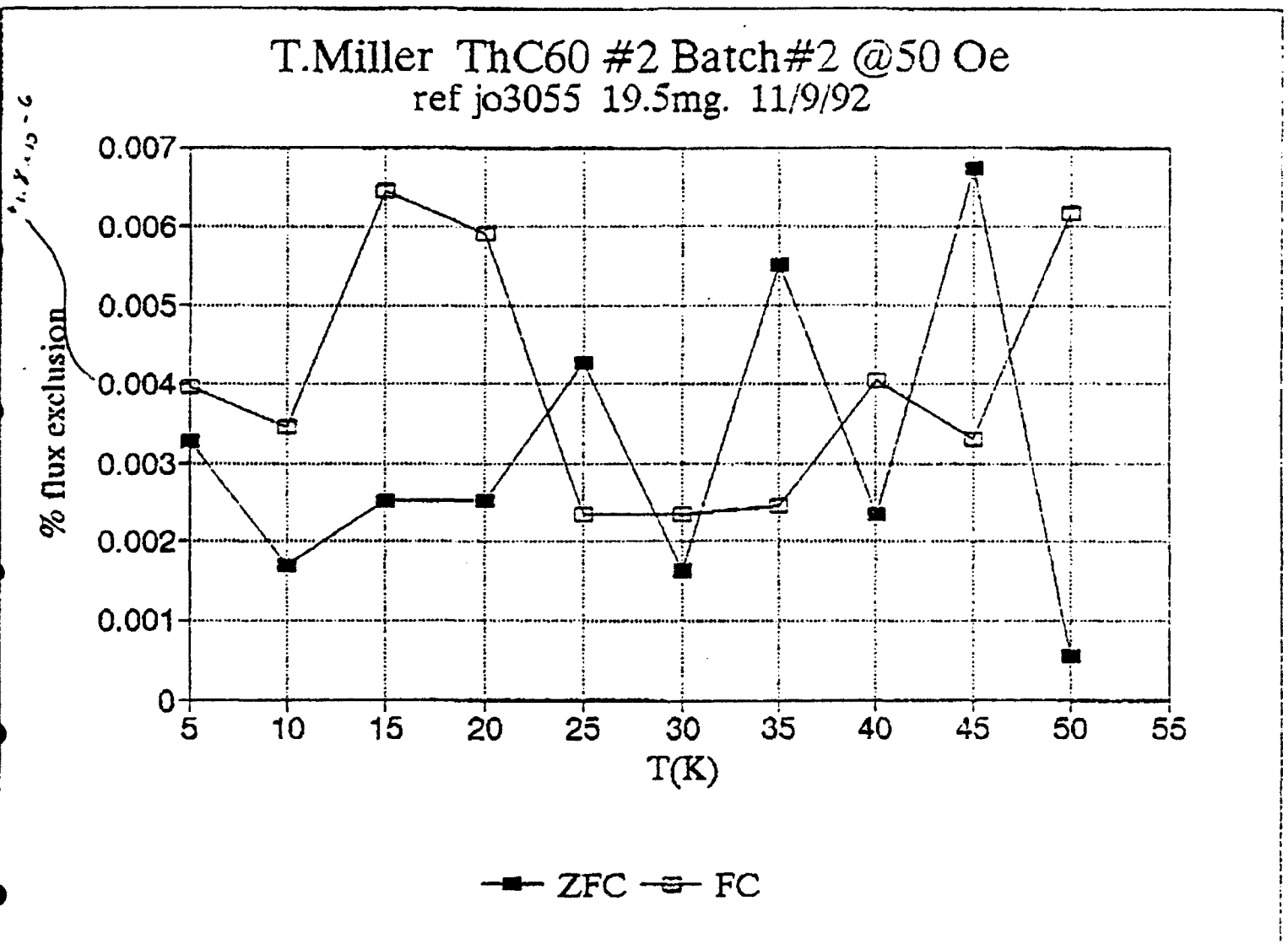


Figure 27. Magnetization of heat treated  $\text{Th}_{15}\text{C}_{60}$  as a function of temperature.

T.Miller ThC60 #4 Batch#1 @50 Oe  
ref jo3058 14mg. 11/10/92

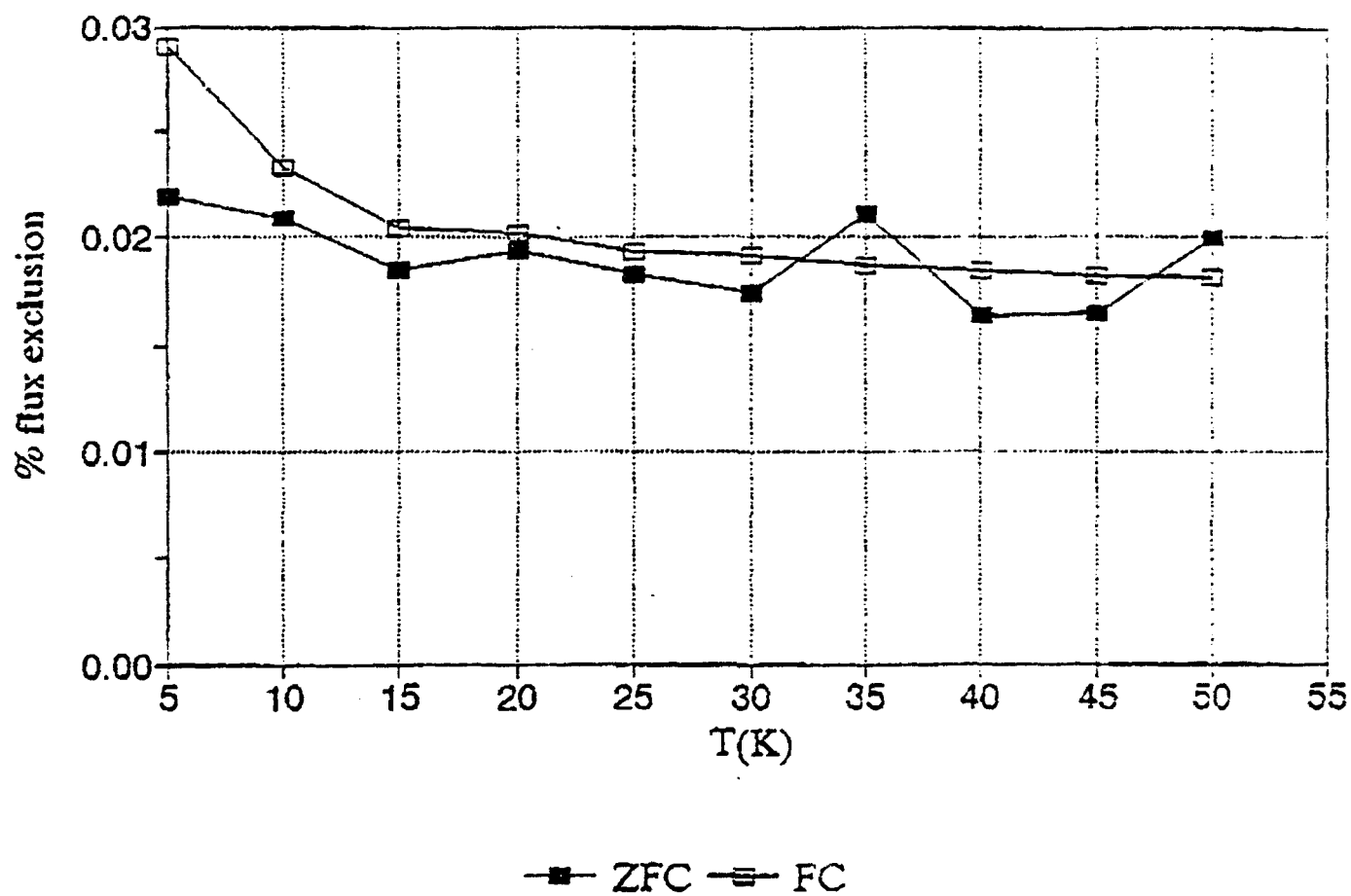


Figure 28. Magnetization of heat treated  $\text{Th}_3\text{C}_{60}$  as a function of temperature.

Of the three Th doped samples,  $\text{Th}_{0.75}\text{C}_{60}$  is the most interesting due to the magnitude of the flux expulsion phenomena and the high magnetic transition temperature. Since the intersection of the zfc and fc curves occurs at the maximum measuring temperature, and since the slopes of the two curves do not join smoothly, it was suspected that the magnetization transition occurred at a higher temperature. Figure 29 supports that suspicion with a magnetization measurement to a higher temperature showing the transition to be at approximately 100 K.

The possibility that the flux exclusion was due to a ferromagnetic transition was tested by measuring magnetic susceptibility below and above the transition. This data is presented in Figure 30 (and Figure 31, expanded by 1000). The data shows an unusual form which was discouraging since at first glance it seems like a ferromagnetic material with a narrow hysteresis (a very small coercivity). But this predominant shape is qualitatively changed very little as the sample goes through the flux exclusion process indicated in Figures 28 and 29. The extremely small coercivity, essentially indistinguishable from the earth's field (for 10K and 150 K measurements especially) indicates that there are two paramagnetic phases, one of which saturates at approximately 1000 Oe, and not a ferromagnetic transition. These predominant features mask indications of a superconducting or ferromagnetic transition and closer inspection is required. Figure 31 shows the magnetization data on an expanded scale illustrating the negligible coercivity of the 10K and 150 K measurement. The 80 K measurement does show trapped flux indicated by the x and y axis intercepts of 20 Oe and 0.4 G respectively. Trapped flux phenomena disappearing at low temperatures is

#9 Batch #3, Th/C60, constriction holder  
jo3099, H= 100 Oe

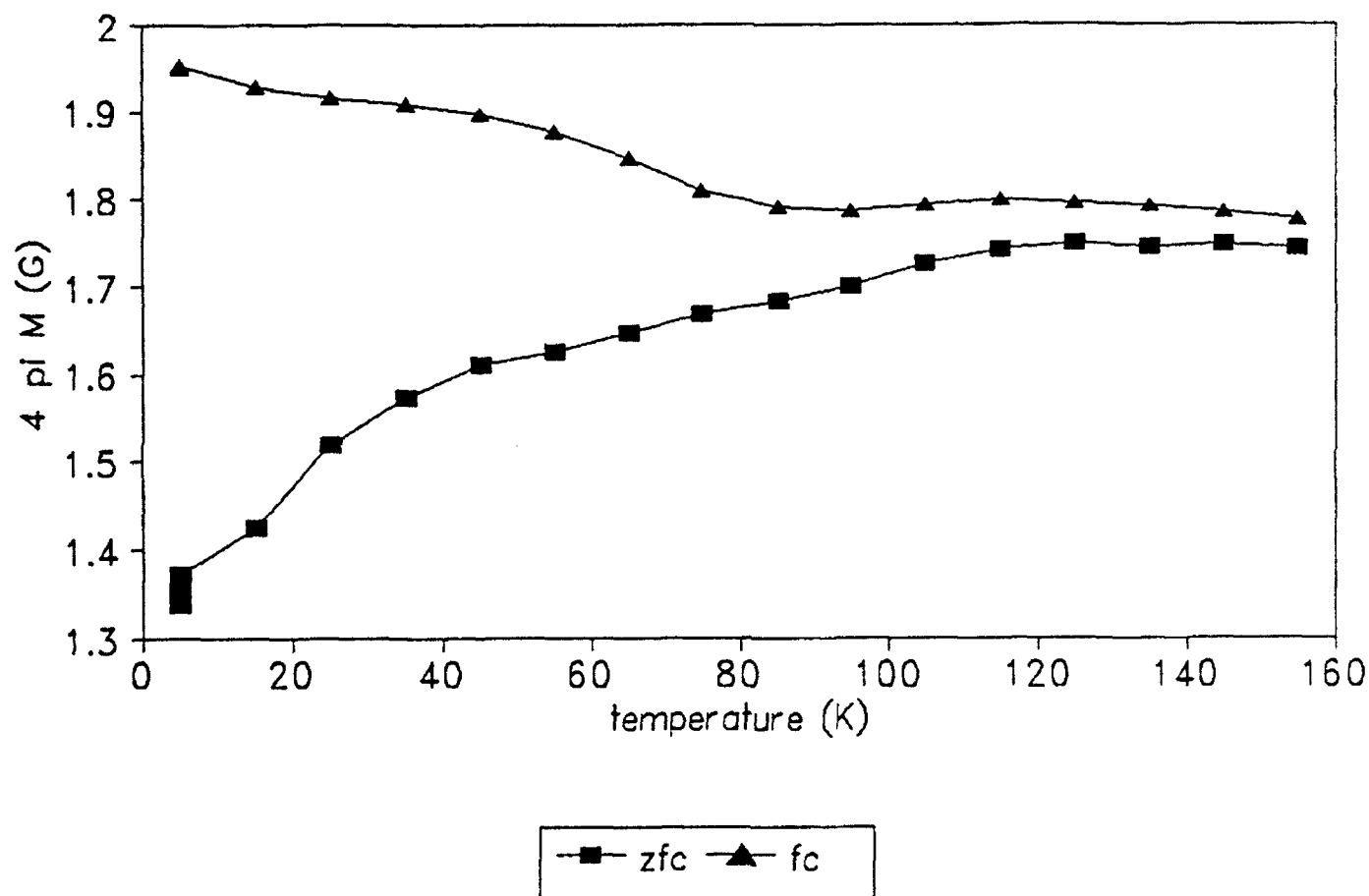


Figure 29. Magnetization of heat treated Th<sub>0.75</sub>C<sub>60</sub> at higher temperatures.

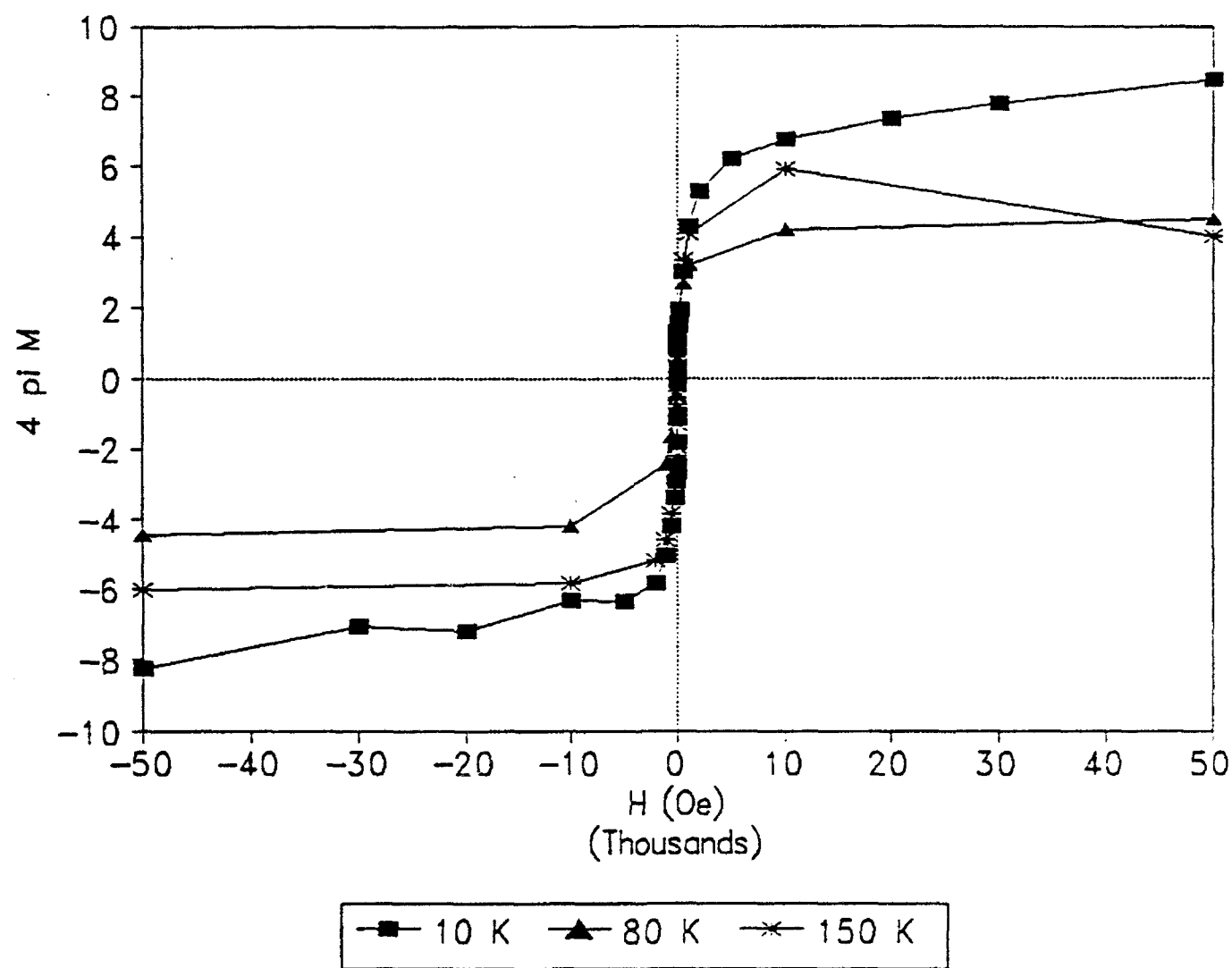


Figure 30. High field magnetization of heat treated  $\text{Th}_{0.75}\text{C}_{60}$  at various temperatures.

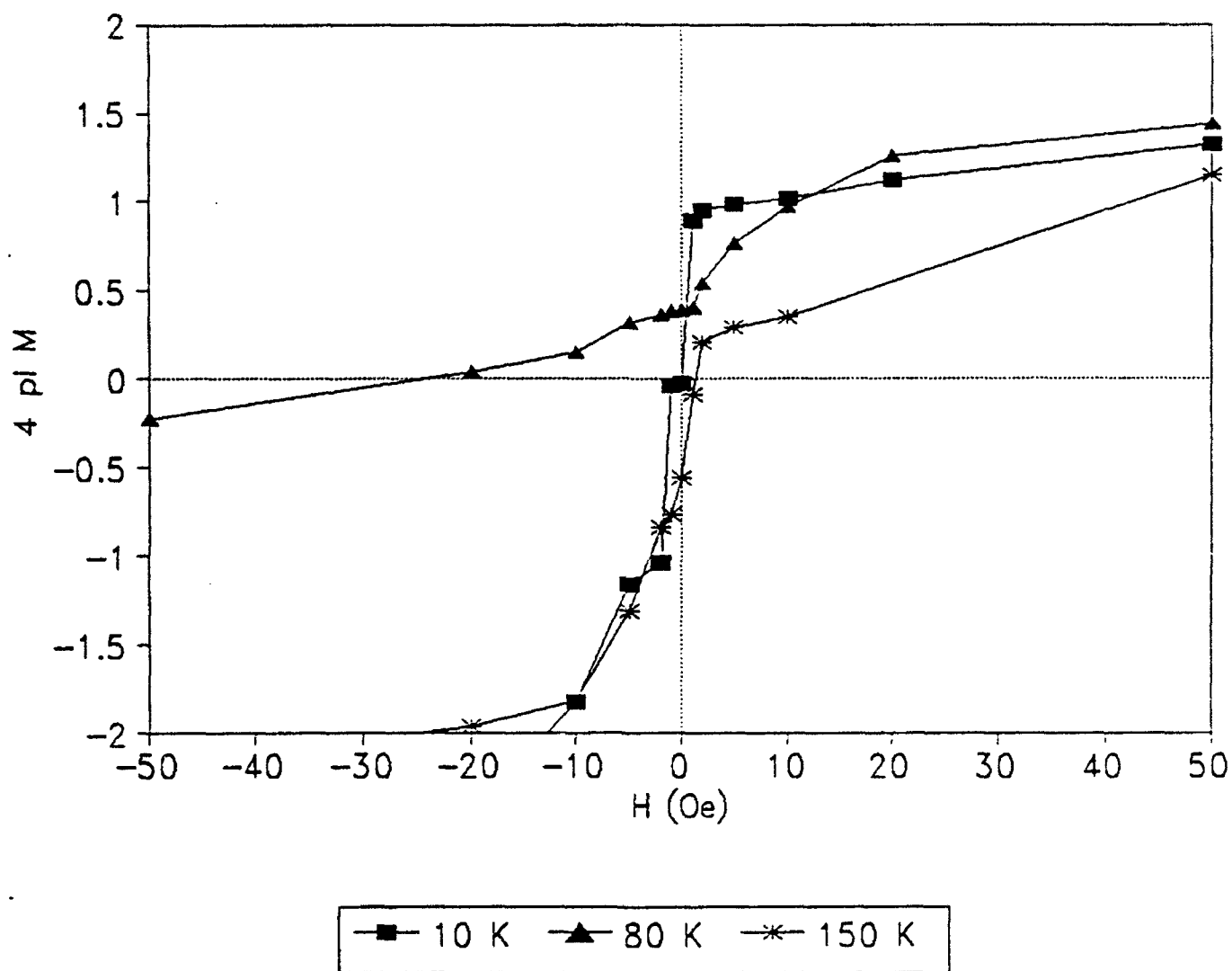


Figure 31. Low field magnetization of heat treated  $\text{Th}_{0.75}\text{C}_{60}$  at various temperatures.

abnormal behavior for a ferromagnet. It is, however, consistent with Type II superconductivity dominating just below the transition temperature, and complete exclusion due to Type I behavior at lower temperatures.

Although the data was measured inconsistently (at different fields progressions) from run to run, we calculated an incremental susceptibility based on this data, shown in Figure 32. Data near zero field ( $< 10$  Oe) is neglected because difficulties in controlling the superconducting magnet at low fields, and because stray fields in the laboratory environment induce widely scattered data. However, the data depicted indicates that the low field susceptibility is lower below the flux exclusion temperature, consistent with an increase in diamagnetism due to superconductivity. This fact is most apparent at 100 Oe, the field used in the magnetization data of Figure 28 and 29.

In summary, because of the small volume percent of the superconducting phase, absolute confirmation of a new superconducting material is not definite. However, all magnetic measurements to date point to superconductivity with a transition temperature of approximately 100 K in this isotropic fulleride, an unprecedented result for fullerene based systems. Additionally, this sample has been handled in the ambient atmosphere, retaining its superconducting characteristics. This material is much more robust than the alkali doped fullerenes, which have been known to be contaminated in reasonably well controlled glove boxes.

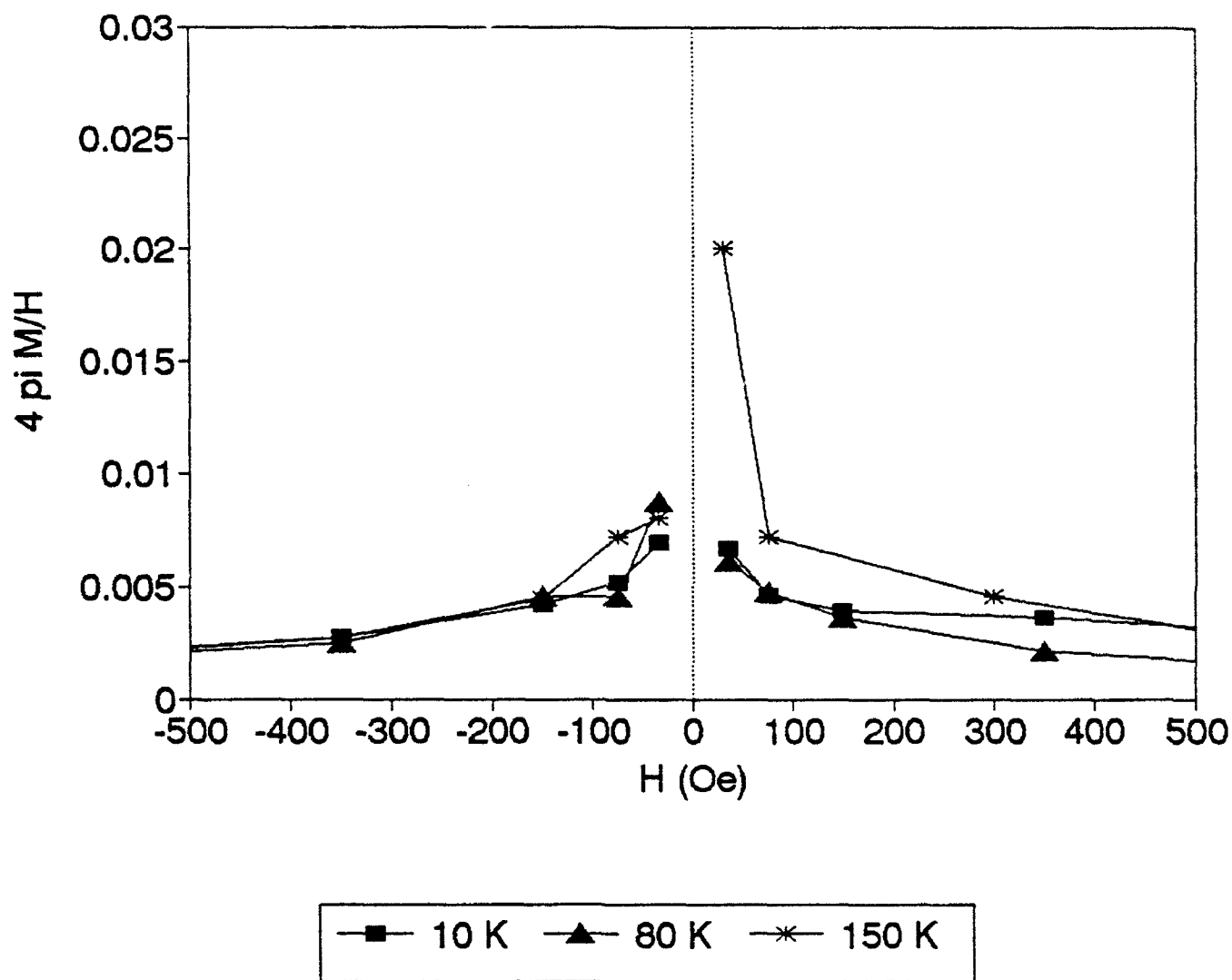


Figure 32. Magnetic susceptibility of heat treated  $\text{Th}_{0.75}\text{C}_{60}$  at various temperatures.

#### IV. Discussion and Conclusion

As is often the case in exploratory research, this project has raised at least as many questions as it has answered. The results will be split into sections on overlayers, on in-cage dopants, and on alternate dopants, as has the rest of the document.

##### A. Protective Overlayers

Thin films of doped fullerenes were prepared. None of the films we prepared in our vacuum system had the resistivity of that reported in the literature ( $2 \text{ m}\Omega\text{-cm}$ ) although some came close. Even though we detected resistance minima as the samples became optimally doped, the minima were generally higher, sometimes much higher than  $2 \text{ m}\Omega\text{-cm}$ . One possibility is that the impurity causing the high resistance is oxygen absorbed during deposition from the background gases in our chamber. Another possibility is that the impurity causing the high resistivities is residual hydroxide from the surface of the potassium pellet that was not eliminated before deposition onto the fullerene film, or hydroxides that are absorbed from the alkaline metals in the glass itself. It is possible that the impurity source is a combination of these effects, but the evidence shown in Figure 8 demonstrates positive evidence that there is some impurity contribution from the background gases in the chamber. Since the resistivity rise shown in Figure 8 was in a vacuum in the  $10^{-6}$  torr range, clearly a UHV deposition system is required with online residual gas analysis for initial manufacturing processes for doped fullerenes.

The impurities both raised the resistivity of the films and prevented superconductivity from occurring at low temperatures. The experiments with the polymer/Al multilayers clearly indicated that 500 Å to 1500 Å of Al was almost sufficient to protect the doped fullerenes. The 5000 Å aluminum overlayer should have completely protected the doped fullerene film. The fact that superconductivity was not observed is likely to be traced in the final analysis to impurities occurring during the deposition process. Fortunately, the multilayer approach did demonstrate the feasibility of using metal, primarily aluminum, as a protective overlayer.

#### **B. In-cage Dopants**

We were successful in incorporating metals into fullerenes as evidenced by the EDS signals in samples extracted from an NMP solution. The magnetometer data from some in-cage samples show the same sort of interesting magnetic transition as the Th alternate dopants samples. The Th doped samples showed a stronger expulsion and were therefore studied more extensively. It is probable that the NMP dissolved material contains many more carbon structures than the metal containing fullerenes. The low level signal problem can be traced to finding a solvent that will separate non-metal-containing fullerenes from metal-containing fullerenes. Our magnetic separation technique showed some promise, but was not pursued because the extreme sensitivity of the DC magnetometer measurements would detect even a small amount of superconducting material. It is probably that metal doped fullerenes could be separated using chromatography since  $C_{60}$ ,  $C_{70}$ ,  $C_{84}$ , etc can be

separated. Alternatively synthesis process development offers the possibility of producing fullerenes in which all fullerenes contain metal dopant.

### C. Alternate Dopants

The samples in this category, particularly the Th doped samples have shown the most tantalizing results of this Phase I project. The magnetometer data indicates a magnetic transition occurring at approximately 100 K. The magnetic transition and flux exclusion can be attributed to a superconducting transition if the the superconducting material phase were a small fraction of the total volume of the material. If the material is a 100 K fullerene-based superconducting phase, then the research of this Phase I project has far exceeded any expectations.

The flux exclusion observed could also be due to a ferro- or ferri- magnetic transition. Examining the magnetic data as closely as possible suggests that, due to a lack of hysteresis at low temperatures, the magnetic characteristics are that of Type II superconductivity at higher temperatures, and Type I superconductivity at lower temperatures. It is difficult to explain a loss of hysteresis at low temperatures in a ferro- or ferri- magnetic system. However, any conclusions as to the superconductivity of a new material based solely on magnetic observations must be carefully interpreted. The matter must be resolved by making samples specifically designed for electrical transport measurements, preferably with a sample pure enough to measure DC resistivity. The thorium doped samples have been handled in the ambient atmosphere, so if it is superconducting, it is important to note that it is ambient atmosphere compatible.